Chapter 2

Synthesis of Perovskite Oxides by Hydrothermal Processing – From Thermodynamic Modelling to Practical Processing Approaches

Juan Carlos Rendón-Angeles, Zully Matamoros-Veloza, Karla Lorena Montoya-Cisneros, Jorge López Cuevas and Kazumichi Yanagisawa

Additional information is available at the end of the chapter

http://dx.doi.org/10.5772/61568

Abstract

The present chapter aims to provide a conscious review of the principles associated with the chemical reactions and the control of the parameters related to the hydrothermal processing of perovskite-structured compounds. Highlights on fundamental principles of the thermodynamic modelling coupled with the relevant technical expertise gained during the past two decades are discussed. Achievements conducted in the early 1990s on thermodynamic modelling of hydrothermal reactions, leading to the estimation of the chemical reaction equilibrium occurring under specific conditions, i.e. above 100°C and 0.1 MPa, are discussed. Additional efforts resulted in different thermodynamic models that predict crystal growth kinetics and the stability for particle nucleation; the models based on chemical population balance approaches are also considered. However, these models do not apply for perovskite compounds containing rare earth elements that crystallize under hydrothermal conditions above 250°C, i.e. orthorhombic lanthanum chromite perovskite. Hence, the final part comprises a literature survey for the experimental research work conducted on various perovskite species produced via hydrothermal treatments, emphasizing the relevant conditions that led to the stoichiometric single-phase crystallization.

Keywords: Perovskite materials, Hydrothermal synthesis, Crystallization, Thermodynamic modelling, Solid-Liquid Equilibrium

1. Introduction

Over the past two decades, remarkable efforts have been conducted worldwide to explore various techniques to prepare perovskite-structured ceramic oxide materials. Perovskite

oxides exhibit a broad variety of functional properties, namely ferroelectricity, piezoelectricity, pyroelectricity and non-linear dielectric behaviour, among others. The functionality of perovskite-structured compounds depends on the relationship established between the specific crystalline structure and the composition of its major constituents. This particular family of inorganic compounds has a large range of interesting physical properties applicable to the design and preparation of different electronic devices with applications in charge storage, non-volatile memories, transducers, actuators and infrared detection. Particular efforts focused on optimizing the physical properties of perovskite-structured compounds have recently taken place by numerous research groups worldwide. Recently, most studies are based on establishing a correlation between the crystalline structure and the chemical stoichiometry of the major constituents. These have led to improvements in the functional properties of the ideal ABX_3 compound with cubic structure (space group).

Another relevant subject that attracted the interest of various research groups concerns with the development of environmentally friendly chemical processes for producing perovskite compounds at laboratory and large scales. The hydrothermal technique has become one of the most suitable chemical processing routes in terms of energy consumption and environmental friendliness for the preparation of a vast number of perovskite compounds with specific crystalline structures and chemical compositions. In the present review, the state-of–the-art associated with this technique is discussed in terms of processing aspects involved in the crystallization of perovskite compounds. In particular for the case of alkaline earth titanate perovskite oxides, these compounds had been used as a standard for developing thermodynamic modelling approaches. These models proposed consider the particular chemical reaction equilibriums that occur under hydrothermal conditions and lead the control of perovskite particle crystallization. Various stability crystallization diagrams were calculated by simulating a complex reaction system containing solid and ionic species in the aqueous phase employing the thermodynamic models. Likewise, a comprehensive analysis is based on the expertise gained during the past two decades by several research groups. With regards to the correlation of the fundamentals principles and the technical aspects involved in the hydrothermal synthesis, a vast number of perovskite compounds are addressed. The present review intends to give guidance for the researchers, as well as to encourage the newcomers from research fields such as Material Science, Chemistry and Physics, by directing their attention towards the key points for conducting hydrothermal reactions for preparing perovskite compounds.

2. Hydrothermal synthesis of perovskite materials

2.1. Structure of perovskite materials, applications and synthesis processes

2.1.1. The crystalline structure of mineral perovskite

The perovskite oxide family has been studied extensively because of the diverse properties exhibited by a material when a considerable number of different atoms produce the typical

http://dx.doi.org/10.5772/61568

atomic arrangement associated with this crystalline structure. Gustav Rose discovered the $CaTiO_3$ mineral in 1839 at the Ural Mountains in Russia, and the mineral was named by the Russian mineralogist Lev Aleksevich Perovski [1]. The "perovskite" term applied to a particular group of inorganic compounds having similar crystalline structure, and the ABX_3 chemical stoichiometry, the major constituent of the compound is $CaTiO_3$. This compound is constituted by divalent (A^{2+}) and tetravalent (B^{4+}) cations. The small B^{4+} cation is corner-sharing bonded with six X^{2-} anions, resulting in an octahedral BX_6 unit forms the ideal face-centered cubic close packed unit cell. Likewise, the large A cation located at the 12-fold coordination sites produces eight octahedral points in the corners of the cube (Figure 1a). In contrast, the simplest atomic arrangement of the ideal cubic cell unit involves a different cation distribution. In this structure the A cations are in the corners of the cube, while the B cation located in the center of the cube is coordinated with six anions in the face-centred positions of the cubic unit cell (Figure 1b). This ideal cubic perovskite is not very commonly found in the mineral reservoirs, because even the mineral species has slight distortions in the atomic ordering in the cubic structure. The study of the perovskite crystalline structure firstly conducted by Goldsmith in 1920 led to propose various fundamental aspects that correlate the crystalline structure and chemical composition parameters [1,2]. One of the most important principles proposed was the tolerance factor. The tolerance factor is one tool normally used for predicting the structural arrangement and stability of a particular perovskite composition, either from the chemical and physical points of view. This factor is evaluated before selecting the adequate processing route for perovskite preparation.

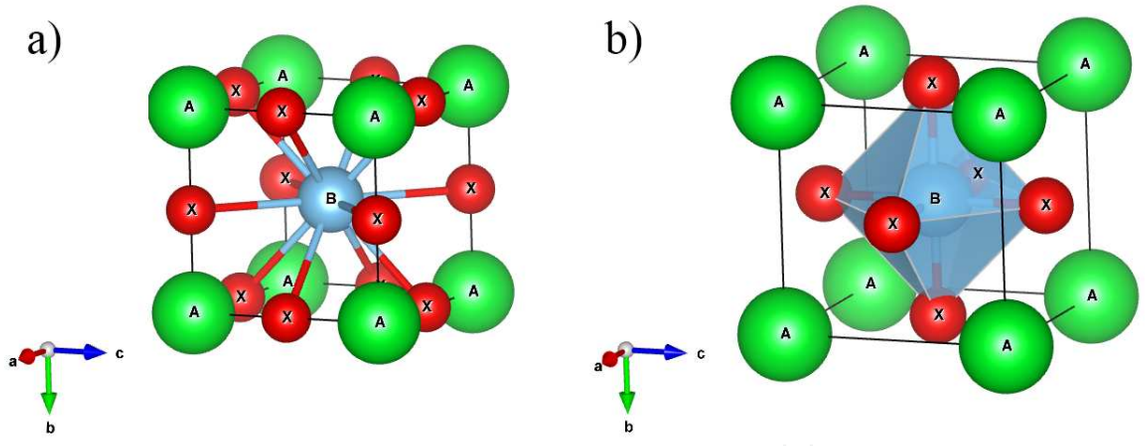

Figure 1. Structural representation of the ideal cubic perovskite showing the (a) cubic A unit cell and (b) cubic B unit cell.

The compounds that belong to the idealized cubic (fcc) structure is $SrTiO_3$ because the strontium titanate oxide exhibits the atomic packing shown in Figure 1b. The ideal cubic structure has a space group. In agreement with the Wyckoff positions, the atomic distribution is as follows: the A atoms are in x, y, z coordinates ½, ½, ½ (Figure 1b) while the B atom is located at 0, 0, 0 (Figure 1b), and the X atoms in 3d are located at spatial positions ½, 0, 0; 0, ½, 0, and 0, 0, ½. The lattice parameter "a_0" of this perovskite structure is 3.905 Å. This crystalline

structure undergoes a series of distortions; one of this is caused by a deficiency in the Sr^{2+} ions (A) in the framework, producing a ReO_3-type structure [2]. Another distortion occurs when the ReO_3 structure transforms into dense packing due to the octahedral unit rotation, producing a structural geometry resembling the hexagonal close packing type, i.e. RhF_3. The void at the centre is in an octahedral surrounding coordination; when this octahedral hole is occupied, the ilmenite structure ($FeTiO_3$) is obtained. The slight distortions attainable in the cubic structure are due to the displacement of ions from the ideal positions, producing a variation of a few tenths of an Å. Therefore, the final symmetry varies considerably between different materials. A mechanism that likely promotes these distortions is related to the capability of perovskite to accommodate a great variety of atoms, due to the flexibility of its crystalline structure [1–3]. An additional mechanism is the Jahn–Teller effect.

2.1.2. Tolerance factor, orthorhombic and hexagonal crystalline unit cells

The ionic radii differences produce the structural distortions on perovskite structure, as was determined in the pioneering research work conducted by Goldschimidt [1–3]. The equation that geometrically correlates the ionic radii (r_A, r_B and r_O) for the ideal cubic cell with the lattice parameter a_0 is given as:

$$a = \sqrt{2}\left(r_A + r_O\right) = 2\left(r_A + r_O\right) \tag{1}$$

The expression that involves the unit cell length ratio is known as the Goldschmidt´s **tolerance factor t**, which is employed to estimate the distortion level attained by a particular perovskite-structured compound. Fundamentally, it considers the ionic radii of the constituent atoms that fit the chemical stoichiometry and enhances a pure ionic bonding between them; the mathematical expression for the tolerance factor is given in Eq. (2).

$$t = \frac{(r_A + r_O)}{\sqrt{2}(r_A + r_O)} \tag{2}$$

According to Eq. (2), the ideal perovskite cubic structure has a "t" value equal to 1, which can be calculated for $SrTiO_3$ with ionic radii of r_A = 1.44 Å, r_B = 0.605 Å and r_O = 1.40 Å. The value of t is less than 1 when the A ionic radius is slightly small, and structurally the octahedral unit [BO_6] tilts forward filling the additional space. From Eq. (2), the grade of tolerance where the ideal cubic structure is attainable in perovskite compounds is $0.89 < t < 1$ [2–4].

Orthorhombic ABO_3 perovskites are among the most important constituents of the Earth´s crust. These compounds have been under exhaustive study due to the wide variety of their functional properties. The distortion of the cubic cell results in the formation of the orthorhombic structure. This process occurs by the tilting of the BO_6 octahedra, but this distortion is not detectable as the temperature increases because the tilt angle decreases [5]. A typical orthorhombic structure that doubles in dimensions the cubic one is shown in Figure 2.

http://dx.doi.org/10.5772/61568

Orthorhombic RMO_3 perovskites (where R = rare earth element or Y, M = 3d-block transition metal) manifests a high intrinsic orthorhombic distortion when the R^{3+} ionic radius is approximately 1.11 Å, and this distortion decreases when the radii of R^{3+} is greater than 1.11 Å. Among the major constituents of the orthorhombic-structured perovskites that have been under exhaustive crystallography studies are $RFeO_3$, $RTiO_3$, RVO_3, $RMnO_3$ and $RNiO_3$. Complementary studies were conducted to determine the correlation between the Jahn–Teller cooperative orbital orderings of M cations with the usual site distortions [6].

The hexagonal-structured perovskite compounds have tolerance factor values above 1. In particular, this occurs when either the A-cation or the B-cation are either too large or too small. The differences on the atomic radii distort the perovskite cubic structure forming the hexagonal perovskites, as it is shown in Figure 2b. In this structure, closely packed layers constituted by octahedra units bonded by face sharing promote the hexagonal structure. The stability of the hexagonal crystalline structure constituted by face-sharing octahedra is lower than that for the one formed by corner-sharing octahedra. However, some hexagonal perovskites belonging to this group overcome this restriction due to the metal–metal bonding between the B ions corresponding to the BX_6 octahedra; these bonds are strong enough so that the metal–metal repulsion is overcome [1]. As a consequence of these stability restrictions, hexagonal perovskites are less commonly found compared with the cubic perovskites. $BaNiO_3$ is one of the hexagonal perovskites that adopt the space group $\boldsymbol{P6_3/mm}$. The representation of the unit cell structure is shown in Figure 2b. This shows the chains of face-sharing BX_6 octahedra orientated along the **c**-axis. Just like the cubic perovskites, hexagonal perovskites can also undergo distortions leading to a variety of structures.

On the other hand, the cubic cell is also susceptible to undergo a small structural deformation producing rhombohedral symmetry, but the deformation does not produce a marked enlargement of the unit cell. Hence, the unit cell likely contains at least one or two rhombohedral polyhedral units with angles of $\alpha \sim 90°$ or $\alpha \sim 60°$. However, the anions are displaced provoking the formation of a large unit cell with $\alpha \sim 60°$.

The tetragonal-structured perovskite, $BaTiO_3$, is probably one known example of a ferroelectric perovskite that is a stable phase at room temperature. In this structure, the TiO_6 octahedra are slightly distorted (one Ti-O bond at 1.86 Å, four at 2.00 Å and a longer one at 2.17 Å). The barium atom is in coordination with four oxygen atoms at 2.80 Å, four at 2.83 Å and four more at 2.88 Å. Another tetragonal perovskites ($PbHfO_3$, $SrPbO_3$, $SrZrO_3$, $AgTaO_3$, etc.) are isotypic with $BaTiO_3$ and possess single-molecular cells. However, a vast number of these materials exhibit the tetragonal structure at elevated temperatures, which makes crystallographic analyses difficult to conduct. In general, a significant number of perovskite-like materials have several polymorphic transformations. Some of these are important regarding their physical properties and applications. The compounds that exhibit this behaviour are $BaTiO_3$ and $KNbO_3$; the following transformation sequence was determined to occur by increasing temperature: rhombohedral → orthorhombic → tetragonal → cubic.

The lowest temperature crystalline compounds (orthorhombic, tetragonal and cubic) have ferroelectric properties. These particular phase transitions are reversible in nature, and all the polymorphic forms exhibit a pseudo-cubic unit cell with $a_0 \sim 4$ Å. Consequently, the polymor-

phic variation on the perovskite structure further affects the crystal chemistry of this group of materials [4–6].

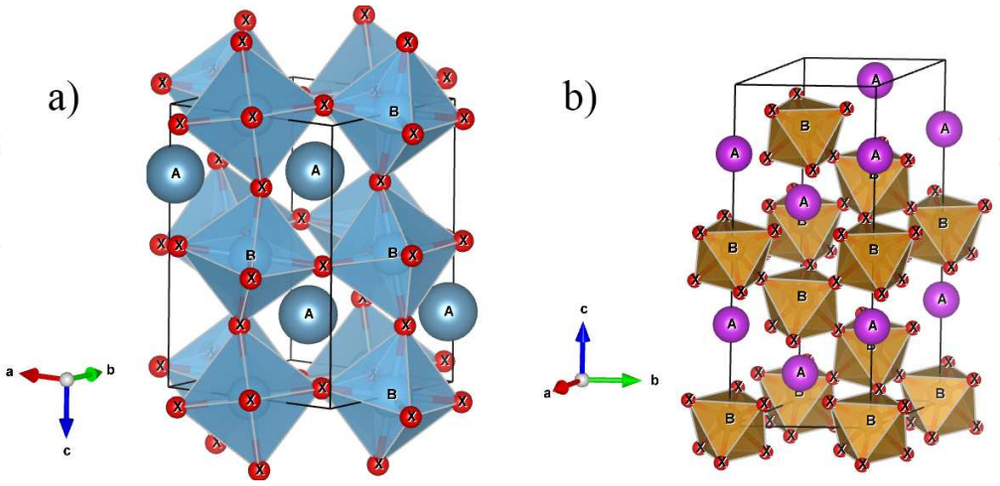

Figure 2. Typical perovskite (a) orthorhombic and (b) hexagonal structural unit cells.

2.1.3. Applications of perovskite materials

Although the physical properties of perovskites-structured materials are not the primary concern of the present review, some relevant ones are discussed below. Since the functionality of perovskites materials was discovered over five decades ago, hundreds of research works have directed forward elucidating the physical and chemical properties of perovskites. These studies have provided pertinent information regarding the fundamentals of the chemical and physical aspects that enhance the structural distortions in ABO_3 materials. The former literature also suggests that there are still surprises to discover for this particular group of compounds, in particular, the perovskites with low tolerance factors; for instance, those comprised in the phase stability diagram $FeTiO_3$-$LiNbO_3$-*Pnma* [7]. A vast number of elements in the periodic table are likely located at either A or B unit cell sites. This fact provides an enormous range of compounds with structural similarity and a variety of properties. Among the most important properties are ferroelectricity ($BaTiO_3$), ferromagnetism (Sr_2FeRuO_6), weak ferromagnetism ($LaFeO_3$), colossal magnetoresistance [8–12], superconductivity ($Ba_{0.6}K_{0.4}BiO_3$) [13] and large thermal conductivity ($LaCoO_3$). Insulating to metallic transitions have a particular interest in the design of devices for thermistor applications ($LaCoO_3$), the fluorescence is applicable for laser devices ($LaAlO_3$:Nd), and transport properties have attracted the attention of research for the development of high-temperature thermoelectric power devices (La_2CuO_4) [1,5,7–14].

Perovskite materials have been investigated for applications involving the preparation of solid electrolytes. The compounds that have been used in various electrochemical devices due to their high performance are barium cerate ($BaCeO_3$) and barium zirconate ($BaZrO_3$). Solid electrolyte performs three essential functions: (1) separates the anode from the cathode in the

http://dx.doi.org/10.5772/61568

electrochemical cell (oxidizing and reducing sides), (2) it can operate as electronic insulator enhancing the flow of electric current through an external circuit and (3) high ionic conduction coefficient, required to provide the control of the electric current flow in the external circuit [15]. Likewise, the proton-conducting ceramics applications are classified according to two basic functions: (1) the material is capable to generate an electromotive force when undergoing a chemical potential gradient and (2) capability for electrochemical ion transport (hydrogen or oxygen) enhanced by an external power source. The employment of an ionic proton conductor as an electrolyte in devices operating under chemical potential gradient provides a device capable of producing electric energy [18,19]. The development of the solid oxide fuel cell (SOFC) electrical power sources was derived from this electrochemical principle. The SOFC is a conversion energy device that generates electricity via an electrochemical reaction occurring at temperatures above 800°C. The chemical reaction that takes place between the fuel (methane, hydrogen, natural gas) and the oxidizing agent (oxygen from air) is the motion to produce the electricity [15,18]. In this particular electrochemical converter device, the principal components responsible for the redox reaction are the electrodes; the ion transport takes place in all the cell constituents (solid electrolyte and electrodes). In contrast with the rechargeable battery devices, the SOFC does not need to be recharged, and it only requires to be continuously fed with a particular fuel for electricity generation [15–20].

Among the miscellaneous applications, such as photocatalytic reactions, some perovskites have been employed. Photocatalytic oxidation was extensively investigated by using various titanates and cobaltites. Titanate perovskite materials ($SrTiO_3$ and $BaTiO_3$) were found to exhibit a strong photocatalytic effect, in contrast with that determined for the easily reducible $LaCoO_3$. Perovskite materials have demonstrated a notable performance as hosts in laser devices because in the A site of the structure some rare earth elements (Nd^{3+} or Sm^{3+}) are incorporated. These elements are some of the major constituents employed to produce laser ion devices. Moreover, various perovskite oxides possess high electrical resistivity, which makes them useful for the preparation of dielectric materials that are poor conductors of electricity, which are widely used for electrical insulation in electrical power systems. Additionally, these materials can be used for energy storage purposes as in capacitors. Typical conductor and semiconductor oxides are characterized to contain either B-ions with a net charge lower than the stable B^{4+}, or B-ions having two different net charges. Typical materials that have been considered to be good conductors or semiconductors are $LaVO_3$, $LaTiO_3$ and $SrMoO_3$. Miscellaneous applications of dielectric perovskites include mechanical actuation, sound generation, in materials subjected to dimensional changes as a result of an applied voltage (piezoelectrics), for transducers as in condensers, for piezoelectric microphones, for detecting changes in temperature as in pyroelectrics, and as liquid crystals employed for alphanumeric displays.

Perovskite oxides materials are also used as oxygen sensors. The mechanism involved in this type of sensors is electrical conductivity in nature, which enhances the oxygen adsorption in the crystalline structure. The electrical conductivity is proportional to oxygen partial pressure and to the concentration of vacant sites in the X site of ABX_3. One compound that exhibits a high sensitivity to oxygen motion is $SrTiO_3$. Furthermore, $SrSnO_3$ is a promising material for

combustion monitoring-sensors. The design of functional materials requires an understanding of the relationship between chemical composition and crystalline structure [15–21].

2.1.4. Synthesis of perovskite materials

The preparation of perovskite oxides has been the subject of considerable research because the design and development of new technological properties require the preparation of materials with special physical morphology. Some examples of the new developments include thin films, porous solids, monodispersed powders with nanometric size, among others. In addition to this, the interest for specific structural ordering exhibiting chains that enhances unidirectional properties has prompted various research groups to pursue the preparation of new perovskite oxides with specific compositions [22,23]. The conventional method of solid-state reaction (ceramic method) was broadly used to produce perovskite oxides powders during the early 1940s. An analogous method, the flux method, which is also based on solid-state reaction, has been employed for the preparation of single crystals of various perovskite oxides [23]. Both methods are adequate to synthesize oxide compounds because they allow achieving the proper conditions in an easy way, due to the reaction proceeding under air atmosphere and ambient pressure [24]. Common steps involved in the solid-state reaction methods are homogeneous grinding and mixing. Oxide and carbonate solid reactants are among the most employed. These are mixed in stoichiometric amounts prior to the conduction of a heat treatment at elevated temperatures (< 1000°C) for long periods of time (several hours or days). The grinding and heating cycles are repeated until the desired pure phase is successfully produced. Any doubt exists in regards of the usefulness and easiness of the universal method, but the achievement of the conditions for atomic diffusion could be a problem. Hence, to accelerate the atomic diffusion for preventing the formation of metastable phases, the process must proceed at high temperatures. However, this has the disadvantage of promoting the volatility of reactants such as lead oxide (in the case of compounds containing Pb^{2+} as in the $PbTiO_3$). In addition, the need of regrinding the materials several times involves high energy and time consumption, as these parameters have a strong influence on achieving the desired product functionality [22–24].

Recently, the solid-state metathesis (SSM) reaction method has emerged as an efficient processing route for synthesizing a broad range of non-oxide compounds. The process occurring under thermodynamic equilibrium conditions is more effective than the conventional solid-state reaction method [22,25]. The SSM reaction method is a variant of the SHS process in which the chemical reactions are conducted very rapidly. A typical SSM reaction involves an ionic exchange taking place between the reactants to produce thermodynamically stable perovskites. Along with the reaction, a remarkable enthalpy change occurs, and high adiabatic reaction temperatures are reached. The solid-state metathesis reaction is conducted using alkaline precursors, chalcogenide, silicide or boride; the salt is reacted with a metal halide according to the general [reaction 3]

$$A_pB_q + CX_p \rightarrow BX_q + pAX \tag{3}$$

http://dx.doi.org/10.5772/61568

where A = Li, Na, K, Mg, Ca, Sr, or Ba; B = B, Si, N, P, As, Sb, Bi, O, S, Se, or Te; C = transition group, principal group or actinide metal, and X = halogen.

The effectiveness of transferring the heat required achieving the chemical reactions under solid-state conditions for the methods mentioned above constitutes one of their main disadvantages from the point of view of the energy cost. One of the new processing techniques that have overcome this problem is the one known as "microwave irradiation". During the microwave processing conditions, the heating is directly supplied to the solid reactants, because it proceeds from the interaction at a molecular level between the electromagnetic field and some of the elements constituting the solid. This interaction varies depending on factors such as the dielectric and magnetic properties of the solid reactants, frequency and microwave power generation, microwave permeability and size and density of the materials [24]. The microwave heating improves the reaction kinetics in a range between 10 and 1,000 folds in comparison with the conventional and the SSM routes, resulting in significant differences associated with the crystalline structure and properties of the reaction products produced. Recently, the synthesis of various perovskite-structured compounds has been under extensive study by microwave processing. Table 1 summarizes the processing details regarding the synthesis of some single-phase perovskite materials produced under microwave irradiation [24].

Chemists in material research are constantly seeking to develop new processing methods with lower costs of energy consumption and that are more environmentally friendly. The novel methods are remarkable functional, allowing us to synthesize perovskite oxides under milder conditions, in comparison with the conventional solid-state process [26–28]. The ceramic materials produced by non-conventional techniques, such as soft chemistry routes, have a more homogeneous distribution of constituents, are purer, can be produced with a wide range of partial dopant substitutions and with various shapes (i.e. coatings and fibers), which are not really obtainable via conventional methods [29]. Soft chemical processing routes also allow the preparation of bulk monoliths without the use of intermediate powders, which occurs by drying a precursor gel at supercritical conditions [29].

Coprecipitation and sol–gel routes emerged since the early 1960s as processing alternatives for ceramic powders, including some perovskite compounds. Certain novelty aspects are inherent in these techniques, which are associated with the control of physical aspects such as size, the state of aggregation and purity of the produced compounds. The functionality of these processes is based on the principles related to the mechanism of formation of colloids in aqueous media at very low temperatures. In the aqueous "sol–gel" processing, the starting chemical reagents, i.e. salt solutions containing specific cation species, undergo chemical treatments at mild temperatures (< 100°C) to form stable colloid dispersions, or sols, when mixed with an acid or basic solution. The particle size of the sols varies between 1 nm and 1 μm. The sols can be prepared from highly hydrolyzable salt reagents such as $ZrCl_4$ or $TiCl_4$, i.e. in the case of perovskite zirconate or titanate. In the "sol–gel" processing, the crystallization step occurs at calcination temperatures much lower than those associated with the preparation of the same crystalline phase via the solid-state process. Prior to this step, the separation of the gel from the sol is conducted by a preliminary dehydration stage [29,30]. Enormous efforts

have been carried out over the past three decades aiming to develop new alternative soft chemistry routes that allow us to reduce the sol–gel crystallization temperature and to control the stoichiometry of the reaction products. One of the processing routes recently proposed involves the reaction of a hydroxide reagent precursor, either NaOH or KOH, with $Nb(OH)_5 \cdot xH_2O$. The dissolution of Nb_2O_5 in an HF solution was the preliminary step to prepare the precursor of niobium. The hydroxide powder mixture containing stoichiometric amounts of the precursor reagents (sources of K and Nb) was heat-treated at different temperatures ranging from 200 to 700°C for 6 h in air. The orthorhombic $KNbO_3$ perovskite phase was produced without the formation of any by-products at a temperature of 700°C while the $NaNbO_3$ powders were prepared at a temperature as low as 500°C [30].

Chemical reagents supplying A and B cations		Reaction product	Microwave		Conventional	
A cation supplier	B cation supplier		Power (W)	Time (min)	Temperature (°C)	Time (min)
Li_2CO_3	Nb_2O_5	$LiNbO_3$	800	15	500	720
Na_2CO_3		$NaNbO_3$	800	17	1,250	*
K_2CO_3		$KNbO_3$	800	12	1,000	1,800
$BaCO_3$	TiO_2	$BaTiO_3$	1,000	25	1,400	*
$PbNO_3$		$PbTiO_3$	600	9	360	480

*Note: Time not specified, the product was obtained after several periods of ball milling.

Table 1. Summary of the processing conditions employed for the preparation of niobate and titanate perovskites via microwave and conventional solid-state processing methods (data taken from reference [24]).

In approaches based on the preparation of polymer precursors using organic solvent solutions, namely the Pechini method and its alternative process polymerized complex method (PC). A polymer containing the cation precursors of the perovskite compound is produced via a chemical reaction occurring between suitable organometallic precursors and the liquid solvent. The polymer precursor is produced by a treatment conducted at low temperature (200–400°C), leading to a compositional homogenization of the elements allocated in the polymer structure [31–33]. The amorphous polymer precursors are usually calcinated to promote the crystallization of the stable $KNbO_3$ [31,32] and $BaTiO_3$ [33] ceramic phases. Furthermore, the polymer precursors can be designed, in terms of their constituents and composition, so as to improve their combustion capability. Based on this principle, a combustion technique has been proposed as a novel soft chemical route. This technique is of industrial interest because it allows processing large batch volumes of powder. Furthermore, the production of nanocrystalline oxide ceramics powders proceeds at lower calcination temperature in a very short time. The produced particles have the highest degree of purity and characteristics such as narrow particle size distribution, higher surface area that enhances its sinterability [32,33]. The combustion technique is based on the exothermic decomposition of

http://dx.doi.org/10.5772/61568

a fuel-oxidant precursor. The reaction promotes the formation of a fine monodispersed powder with perovskite structure, or a partially decomposed precursor containing considerable amounts of carbon traces. The results after processing depend on the precursor and in the fuel-to-oxidant ratio used to conduct the combustion. During the decomposition, the decomposition of the organic compound facilities the rapid increase of the temperature coupled with gas production, resulting in the coalescence of particles inconsequence short diffusion pathways as well. Hence, a foamed porous aggregate formed by a pure-phase nanoparticles agglomerated can be obtained at low temperatures [32,33].

Miscellaneous processing techniques involving non-equilibrium reaction conditions are also of industrial interest to produce perovskite oxides. The glycothermal method is a novel technique involving crystallization of oxide particles, i.e., $KNbO_3$, and which is conducted at supercritical conditions, depending on the chosen organic solvent. At supercritical conditions, the organic solvent capability is similar to that of the normal polar liquids, but it exhibits better transport properties (viscosity, diffusivity and thermal conductivity, among others) [34]. This technique is reliable in terms of reproducibility and environmental aspects. However, the high cost of the organometallic reagent precursors and the restricted types of organic solvents are some disadvantages associated with this technique. An analogous technique that employs only water as the solvent, hydrothermal processing has been widely used for more than three decades to synthesize a numerous variety of perovskite materials. This technology was explored in the engineering fields of crystal growth and metal leaching in the middle of the 20th century. Hitherto, the hydrothermal technology broadly covers various interdisciplinary fields of materials science. In the solid-state chemistry field, the hydrothermal media have recently been exploited for preparing vast type of ceramic compounds. This technology provides an efficient reaction environment for synthesizing perovskite powders, due to the effect of a combination of parameters, such as solvent media, temperature and pressure, on the ionic reaction equilibrium. The conventional hydrothermal (CH) method is an efficient route that enhances the crystallization of micro/nanometric morphology controlled and crystal growth-oriented particles. In addition to that, this method depends on the inorganic salts solubility in water under variable temperature and pressure conditions. Another fundamental factor that has a marked influence enhancing the heterogeneous reactions in this process is the vapour pressure. Hence, a detailed state-of-the-art regarding this technique is discussed in the next sections. A particular emphasis that considers the theoretical principles associated with thermodynamic modelling of the heterogeneous chemical reaction equilibrium associated with a particular hydrothermal environment is addressed. Additionally, the link between the theoretical principles and the extensive practical expertise gained over the past decades regarding the hydrothermal synthesis of the most representative perovskite compounds is further discussed in the final section of the present review.

2.1.5. Definition of hydrothermal synthesis

The word “hydrothermal” comes from the etymological root of the Greek word “hydrous” that means water while “thermal” means heat. The “hydrothermal” term has a purely

geological origin. In the middle of the 18th century, the Scottish Geologist Sir Roderick Murchinson introduced this term to the Scientific Society. In practical terms, he described that the formation of mineral species that occurred on Earth's crust is due to the reaction of water exposed to conditions of elevated temperature and pressures. Another technical definition accepted by the Scientific Society refers the "hydrothermal" term as any heterogeneous chemical reaction, occurring in the presence of a solvent media. The reactions occur inside a hermetical sealed vessel system at temperatures above 25°C and pressure of 0.1 MPa. Under hydrothermal conditions, it does not matter whether the solvent is aqueous or non-aqueous. The crystallization process of solid phases under hydrothermal conditions is carried out at autogenous pressure, achieved by the saturated vapour pressure of the fluid at the specified temperature and composition of the hydrothermal solution. In this concern, in terms of industrial and commercial processing, mild operating conditions are preferred, for example, temperatures of treatment below 350°C and pressures less than 50 MPa [35, 36]. The processing parameter that allows the transition from mild to severe reaction conditions during a hydrothermal treatment is the lining material strength of the autoclave vessel. At severe treatment conditions in highly concentrated acidic or basic solutions, the lining material might undergo a rapid corrosion process. The progress in the experimental work research in this area of investigation has allowed improving the understanding of how is the behaviour of the chemical reactions generated in the hydrothermal media. The crystallization of several materials of oxide and non-oxide has been made with adequate optimization of the experimental parameters during the hydrothermal treatment ($T < 200$°C and $P < 1.5$ MPa). The recent scientific and technological achievements have made the hydrothermal synthesis more economical. One example is the synthesis of ceramic particles, which can be prepared in a single step, using advanced pressure reactor technology coupled with processing methodologies proposed for a wide number of inorganic compounds [37].

2.2. Thermodynamic modelling associated with the hydrothermal synthesis of perovskite oxides

In the early 1990s, a great interest to prepare monodispersed perovskite oxide fine particles with controlled morphology was the main concern of the chemical community. One chemical technique that provides an adequate environment to accomplish the preparation of a substantial number of ceramic materials is the hydrothermal processing. Because this method combines the dynamic interaction of processing parameters such as solvent type, temperature and pressure that governs the ionic mobility, this particular technique involves numerous simultaneous chemical reactions, which normally take place in an aqueous system comprising the interactions of dissolved and solid species. The reaction product obtained consists of an anhydrous single-phase crystalline oxide or multicomponent phases. The huge diversity of precursor chemical reactants (i.e. water, soluble salts, hydroxides and oxides, among others) allows preparing solvents that can be employed as hydrothermal media. This processing parameter promotes a broad range of reaction pathways to achieve the crystallization of a solid in a particular hydrothermal reaction system. In general, phase-pure oxides (perovskite-structured) with specific stoichiometry, particle size and morphology can be hydrothermally

http://dx.doi.org/10.5772/61568

produced in one step processing, even using low-cost reagents at mild temperatures and pressures, five-fold lower than those required for conventional processing techniques.

Hitherto, the practical fundamentals derived from the expertise gained over the past five decades. Regarding the processing of inorganic compounds by the hydrothermal technology, to take an adequate advantage of the technology´s novelty, one must bear in mind some critical key processing factors such as the selection of a suitable precursor system (highly reactive and cost-effective) required for the optimization of the chemical equilibrium that enhances the crystallization of the desired phase. The effectiveness of the selected experimental approach can be evaluated selecting the suitable chemical precursor concentration and mixing ratios, pH of the hydrothermal media, temperature and pressure level [38,39]. This procedure is relatively complex and time-consuming due to the numerous variables involved. Hence, to determine the effectiveness of the precursor hydrothermal system, an approach based on thermodynamic modelling to simulate the hydrothermal reactions has been developed since the early 1990s [40]. OLI Systems Inc. (USA) developed an algorithm that included the thermodynamic basis to simulate the chemical reactions. The model is capable to calculate thermochemical data with high consistency and accuracy for a broad number of perovskite compounds, including the single-phase $CaTiO_3$, $SrTiO_3$, $SrZrO_3$, $PbTiO_3$, $BaTiO_3$, as well as some selected solid solutions of $Ba_{1-x}Sr_xTiO_3$ and $PbZr_{1-x}Ti_xO_3$ [41–49]. In addition to that, these studies have produced relevant information regarding the behaviour of solutions under modifying pressure and temperature conditions. The most features investigated under hydrothermal conditions are solubility, stability and yield product amount, reaction mechanisms, among others.

2.2.1. Thermodynamic model

Today, our knowledge of the physical chemistry of the hydrothermal processes is enriched by the experience acquisition in the area of hydrothermal solution chemistry. The role of the solvent during the hydrothermal treatment needs to be understood because it depends on the experimental variables temperature and pressure. Also, the solvent reactivity is affected under hydrothermal conditions by some interrelated parameters such as the structure at critical, supercritical and subcritical conditions, dielectric constant, pH variation, viscosity, coefficient of expansion and density. In general, the thermodynamic modelling applied to a hydrothermal system constitutes a potential tool for predicting the concentration and activities of ionic or neutral substances used as solvents. These include a reaction system constituted for some solid, vapour and non-aqueous phases. A particular methodology involving a model based on the theory of electrolyte systems is established; the model enables a quantitative description of both the phase and the ionic equilibrium and provides values of the activity coefficients. Furthermore, the models provide data about the standard-state properties of all the substances involved in the reaction model, coupled with the Gibbs energy excess (referred to a non-ideal solution). Rafal and Zemaitis have given a complete interpretation of the experimental design fundamentals for thermodynamic modelling of the hydrothermal systems, as described in Ref. [39].

The hydrothermal medium is an environment for the inorganic particle synthesis. The chemical interactions between solid and fluid phases are affected mainly by variables such as solvent liquid, temperature, reaction interval, pH of the solvent fluid, the initial concentration of the precursor feedstock and occasionally pressure. The correct selection of these parameters is crucial to determinate the principal production conditions that allow the formation of single-phase stoichiometric compounds, namely ABX3. Pioneering hydrothermal research investigations were conducted empirically, establishing the experimental parameters in a trial-and-error fashion, resulting in an inaccurate approximation for a practical particle synthesis. The hydrothermal reaction system becomes complex when highly concentrated solutions rich in ions are employed, or if multiple heterogeneous chemical reactions alternatively proceed in the hydrothermal media. In this particular case, the ionic concentration related to the chemical equilibrium promoted in the hydrothermal fluid is strongly dependent on ionic species activity coefficients [38]. At the early 1990s, Lenka and Riman reported the first rigorous approach that is in essential a practical thermodynamic model of ionic species hydrolyzed in a hydrothermal reaction system [40]. The model is capable of predicting or optimizing the experimental conditions, namely feedstock composition, solution pH, temperature and pressure, to minimize the Edisonial trial and error design. Additionally, this model produces a series of phase stability diagrams based on the interaction of the main parameters, such as feedstock concentration, solvent pH and its concentration.

The parameters required to obtain a hydrothermal phase stability diagram are the equilibrium concentrations of the ionic species added in the system as a function of temperature, pressure and the initial content of the precursor feedstock. Initially, the number of independent chemical reaction equilibria produced under hydrothermal conditions is denoted by "*k*". The specific jth reaction ($j = 1,..., k$) imply n_j different chemical substances; these are represented by $A_i^{(j)}$ ($i = 1,..., k$). Thus, the number of possible reactions occurring in an infinitesimal point in the hydrothermal system can be given by the following expression 4.

$$\sum_{i=1}^{n_j} v_i^{(j)} A_i^{(j)} = 0, \qquad j = 1,\ldots\ldots k. \tag{4}$$

While the equilibrium state of any *j*th reaction is determined using the expression for the variation in the standard Gibbs energy

$$\Delta G_j^0 = \sum_{i=1}^{n_j} v_i^{(j)} \Delta G_f^0\left(A_i^{(j)}\right) = -RTlnK_j\left(T,P\right), \qquad j = 1,\ldots k. \tag{5}$$

Where $G^0(A_i^{(j)})$ corresponds to the standard Gibbs energy for the substances formation ($A_i^{(j)}$) and K_j represents the equilibrium constant of the *j*th reaction.

The equilibrium constant of any reaction is related to the molality "*m*", which is the used concentration unit. This can be expressed as

http://dx.doi.org/10.5772/61568

$$K_j(T,P) = \prod_{i=1}^{n_j} \left(m_{A_i^{(j)}} \gamma_{A_i^{(j)}} \right)^{v_i^{(j)}}, \qquad \left(j = 1,\ldots,k\right) \tag{6}$$

where $\gamma_{A_i^{(j)}}$ represents the activity coefficient of the ionic species $A_i^{(j)}$. To solve Eqs. 4 and 5, the mass and electro neutrality equilibria must be established, coupled with the standard Gibbs energy values associated to the formation and activity coefficients. In parallel to the solution of these equations, the Helgeson-Kirkham-Flowers-Tanger (HKFT) equation of state must be taken into account. The HKFT equation provides the standard-state thermodynamic functions of aqueous, ionic and neutral species as a function of both temperature and pressure up to 1000°C and 500 MPa, respectively. In addition, the values of the standard Gibbs energy of formation are calculated from the standard Gibbs energy, ΔG_f^0 enthalpy ΔH_f^0 of formation and entropy S^o at a reference temperature (usually, 25°C, 298.15 K). Furthermore, parameters that must be considered are the partial volume V^o and the heat capacity C_p^0 as functions of temperature. The algorithm OLI Systems Inc employs a Debye-Hükel term for net ionic species interactions, a modified Bromley expression (Bromley-Zemaitis) for a short-range ionic interactions and the Pitzer expression of ion-neutral molecule interactions (as described in detail in Ref. [38]). Some restrictions in the use of the Pitzer term are taken into account in a simplified version of the model algorithm, and also without considering three-body interactions. The OLI software data bank contains vast information associated with the standard thermodynamic values for several liquids, gaseous and solid substances; data from other sources should strictly be evaluated before using them. The information of solid substances is obtained from the JANAF/NBS databases, as well as from some other particular references such as Medvedev [43] and Robie [44] in Ref. [38]. For the case of ceramic materials, especially perovskite oxides, i.e. lead and alkaline-earth titanates, thermochemical data of pure substances have been reported by Brain [40].

Solubility databases of solid species in pure water and other solutions, namely alkaline and/or acidic solutions, as a function of temperature, are the best reference data to obtain the standard-state properties. These data can be taken from the books Thermochemical Data of Pure Substances and Solubilities of Inorganics and Metal Organic Compounds (Refs. 45 and 46 in Ref. [38]). However, precise and accordant thermochemical data regarding the solubility of solid compounds can be obtained by regression fitting performed using the OLI software [38,40].

The methodology proposed by Lenka and Riman [38] to determine the chemical reaction equilibria is associated with a set of feedstock precursors. For example, an organic salt (barium acetate) or an inorganic salt (barium nitrate) and an oxide containing a tetravalent cation are used for the preparation of a double cation perovskite oxide (ABX_3). The set of chemical reactions that are likely to occur in the hydrothermal process are summarized in Table 2. This table contains the equilibria equations of 37 aqueous and solid substances that might prevail in the Ba-Ti-H_2O system. One fact that deserves emphasis is related to the usage of HNO_3 and KOH because the addition of acidic or alkaline reagents is required to control the pH of the

hydrothermal fluid. The presence of these solutions strongly affects the crystallization of the oxide species. The most common reagents employed to adjust the pH of the hydrothermal reaction media are alkaline solutions, such as hydroxide solutions and ammonia. In order to complete the set of modelling data, the gaseous species produced during the hydrothermal treatment needs to be calculated as well. In general, for the synthesis of perovskite compounds under specific T–P conditions, the gaseous species play a secondary role in their formation. It is necessary to remark that even a relatively simple hydrothermal system (Ba-Ti-H_2O) includes a vast variety of species, which lead to the formation of a lot of equations for resolving.

The estimated entropies corresponding to the possible reactions in the hydrothermal medium are given in Table 3. Once thermodynamic parameters are determined at room temperature condition, their values at different conditions must be determined using the approach described in Ref. [40]. The complete set of data referring to the ionic species standard-state properties are used to obtain the Ba-Ti system stability diagram. The data show the predominant phases at the conditions of T and pH as a function of the net content of Ba $\left(m_{Ba_T}\right)$ or Ti $\left(m_{T\,i_T}\right)$. The standard-state values of all the species involved in the reaction system are calculated assuming that inner pressure in the hydrothermal vessels is autogenously controlled.

The iterative practice of the model using different A and B site feedstock concentrations, in conjunction with the addition of pH adjusting agents (mineralizer or solvent), allows to estimate diagrams that correlates product yield and crystalline phase stability.

$H_2O = H^+ + OH^-$	$Ba(CH_3COO)^+ = Ba^{2+} + (CH_3COO)^-$
$H_2O_{(g)} = H^+ + OH^-$	$Ba(CH_3COO)_{2(aq)} = Ba(CH_3COO)^+ + (CH_3COO)^-$
$TiO_{2(s)} + OH^- = TiOH^{3+} + H^+$	$Ba(CH_3COO)_3{}^{2-} = Ba^{2+} + 3(CH_3COO)^-$
$Ti^{4+} + H_2O = TiOH^{3+} + H^+$	$Ba(CH_3COO)_{2(s)} = Ba^{2+} + 2(CH_3COO)^-$
$TiOH^{3+} + H_2O = Ti(OH)_2{}^{2+} + H^+$	$BaNO_3{}^+ = Ba^{2+} + NO_3{}^-$
$Ti(OH)_2{}^{2+} + H_2O = Ti(OH)^{3+} + H^+$	$Ba(NO_3)_{2(aq)} = BaNO_3{}^+ + NO_3{}^-$
$Ti(OH)^{3+} + H_2O = Ti(OH)_{4(aq)} + H^+$	$Ba(NO_3)_{2(s)} = Ba^{2+} + 2NO_3{}^-$
$Ti(OH)_{4(aq)} = TiO_{2(s)} + 2H_2O$	$HCH_3COO_{(g)} = HCH_3COO_{(aq)}$
$TiO_{2(rutile)} + 2H_2O = Ti(OH)_{4(aq)}$	$HCH_3COO_{(aq)} = H^+ + (CH_3COO)^-$
$TiO_{2(anatase)} + 2H_2O = Ti(OH)_{4(aq)}$	$(CH_3COO)_{2(aq)} = 2HCH_3COO_{(aq)}$
$Ba(OH)_{2(s)} = Ba^{2+} + OH^-$	$(CH_3COO)_{2(vap)} = (CH_3COO)_{2(aq)}$
$BaO_{(s)} + 2H^+ = Ba^{2+} + H_2O$	$HNO_{3(g)} = HNO_{3(aq)}$
$CO_{2(g)} = CO_{2(aq)}$	$HNO_{3(aq)} = H^+ + NO_3{}^-$
$CO_{2(aq)} + H_2O = H^+ + HCO_{3-}$	$KOH_{(s)} = K^+ + OH^-$
$HCO_{3-} = H^+ + CO_3{}^{2-}$	$KOH_{(s)} \cdot 2H_2O = K^+ + OH^- + 2H_2O$
$BaCO_{3(s)} = Ba^{2+} + CO_3{}^{2-}$	$KCH_3COO_{(aq)} = K^+ + (CH_3COO)^-$
$BaHCO_{3+} = Ba^{2+} + HCO_3{}^-$	$KNO_{3(aq)} = K^+ + NO_3{}^-$
$BaTiO_{3(s)} + H_2O = Ba^{2+} + 2OH^- + TiO_{2(s)}$	$KTiO_{3(s)} + 3H_2O = 2K^+ + Ti(OH)_{4(aq)} + 2OH^-$
$Ba_2TiO_{4(s)} + 2H_2O = 2Ba^{2+} + 4OH^- + TiO_{2(s)}$	

Table 2. Reaction equilibria in the Ba-Ti-H_2O hydrothermal system using TiO_2, $Ba(CH_3COO)_2$ and/or $Ba(NO_3)_2$ as precursor feedstock [38,40].

http://dx.doi.org/10.5772/61568

	Ionic species						
	H^+	$BaOH^+$	$BaHCO_3^+$	Ba^{2+}	Ti^{4+}	$Ti(OH)^{3+}$	$Ti(OH)_2^{2+}$
ΔG_f^0 /(kJmol^{-1})	0	-716.72	-1153.5	-560.78	-354.18	-614.0	-869.56
ΔH_f^0 /(kJmol^{-1})	0	-749.35	-1207.2	-537.64	-	-	-
S^0 /(Jmol^{-1}K^{-1}	0	55.5	195.9	9.62	-456.5	-189.85	-40.8
C_p^0 /(Jmol^{-1}K^{-1})	0	44.0	-	-12.3	-	-	-
10^6 V^0/(m^{3}mol^{-1})	0	-	-	-12.6	-	-	-
lit.	0	14, 21	16	16, 21	14, 21	14, 39	14, 39

	Ionic species				
	$Ti(OH)_3^+$	OH^-	CO_3^{2-}	HCO_3^-	$HTiO_3^-$
ΔG_f^0 /(kJmol^{-1})	-1092.5	-157.30	-527.98	-586.94	-955.88
ΔH_f^0 /(kJmol^{-1})	-	-230.03	-675.23	-689.93	-
S^0 /(Jmol^{-1}K^{-1})	56.9	-10.7	-50.0	98.4	117.3
C_p^0 /(Jmol^{-1}K^{-1})	-	-	-290.8	-35.4	-
10^6 V^0/(m^{3}mol^{-1})	-	-	-21.0	102.9	-
lit.	14, 39	11	16, 21	16, 21	38

	Aqueous species			
	H_2O	$Ti(OH)_4$	CO_2	$BaCO_3$
ΔG_f^0 /(kJmol^{-1})	-237.25	-1118.38	-385.97	-1103.9
ΔH_f^0 /(kJmol^{-1})	-285.83	-1511.26	-413.8	-1196.0
S^0 /(Jmol^{-1}K^{-1})	70.0	-54.8	117.6	66.9
C_p^0 /(Jmol^{-1}K^{-1})	75.3	-50.2	243.1	-
lit.	11	14	16, 22	16

	Solid species			
	$Ba(OH)_2$	$BaCO_3$	$BaTiO_3$	BaO
ΔG_f^0 /(kJmol^{-1})	-855.17	-1164.8	-1572.4	-525.35
ΔH_f^0 /(kJmol^{-1})	-941.40	-1244.7	-1659.8	-553.54
S^0 /(Jmol^{-1}K^{-1})	108.8	112.1	107.9	70.4
C_p^0 /(Jmol^{-1}K^{-1})	97.9	-	102.5	-
a /(Jmol^{-1}K^{-1})	116.8	89.96	121.5	53.30
10^3 b/(Jmol^{-1}K^{-2})	18.44	46.28	8.535	4.351
10^{-5} c/(Jmol^{-1}K)	-18.41	-16.36	19.16	8.301
10^6 V^0/(m^{3}mol^{-1})	38.19	45.81	38.80	25.59
lit.	14, 13b, 43	16	15, 41, 37	15, 41, 44

	Solid species			
	$Ba(OH)_2 \bullet 8H_2O$	Ba_2TiO_4	$TiO_2(rutile)$	$TiO_2(anatase)$
ΔG_f^0 /(kJmol^{-1})	-2779.9	-2132.9	-890.70	-883.27
ΔH_f^0 /(kJmol^{-1})	-3328.4	-2243.0	-946.01	-938.92
S^0 /(Jmol^{-1}K^{-1})	422.6	196.6	50.3	49.9
C_p^0 /(Jmol^{-1}K^{-1})	-	-152.6	55.1	-55.3
a /(Jmol^{-1}K^{-1})	-	179.9	62.85	75.04
10^3 b/(Jmol^{-1}K^{-2})	-	6.694	11.38	0.0
10^{-5} c/(Jmol^{-1}K)	-	-29.12	-9.897	-17.63
10^6 V^0/(m^{3}mol^{-1})	144.7	-	18.82	20.52
lit.	14, 45	15, 41	16	15, 42, 44

Table 3. Relevant species in the Ba-Ti hydrothermal systems and their standard state properties at 25°C (298.15 K).

2.2.2. Stability diagrams calculated from the thermodynamic model

The stability diagrams have been developed for a vast number of hydrothermal systems including those research works related to the preparation of double component oxides. The stability diagram of perovskite-structured compounds, single-phase stoichiometry ABX_3 [41–47] and some relevant solid solutions [48, 49] are the most investigated applying thermodynamic modelling under hydrothermal conditions. Stability diagrams supply pertinent information regarding the ranges of equilibrium conditions at which several aqueous and/or solid species are stable in the hydrothermal reaction system. The molality of the aqueous ionic precursor includes the sum of equilibrium concentrations corresponding to dissolved ionic species in the hydrothermal media, but this term does not take into account the ionic species that precipitate from the solution. The stability diagrams also provide details related to the optimum conditions enabling incipient crystallization of the solid phases involved in the reaction. This process occurs when the ionic constituents that form the solid phase reach the supersaturation conditions in the hydrothermal fluid promoting its nucleation. However, the determination of the experimental reaction conditions required for an assumed yield of a perovskite reaction product from these diagrams is not straightforward.

The diagrams are constituted for two fields, as can be seen in Figure 3a: the solid lines indicate the boundary of incipient solid crystallization while the dashed lines denote the location where two ionic species in the liquid have equal concentrations. The stability phase diagrams are usually calculated solving the equilibrium and balance equations for the compositions of starting feedstock that accounts for the total Ba (m_{Ba_T}) as function of pH or Ti ($m_{T\,i_T}$) as function of pH, respectively. Typical examples of these diagrams calculated for the Ba-Ti-H_2O system were produced at two different temperatures, 25 and 90°C. The latter temperature has been empirically determined to correspond with optimum for the hydrothermal processing of perovskite particles of $BaTiO_{3(s)}$ [40]. In this typical example, the stability diagrams were calculated at 25°C (lines 1) and 90°C (line 2) by using an ideal approximation, the approach

http://dx.doi.org/10.5772/61568

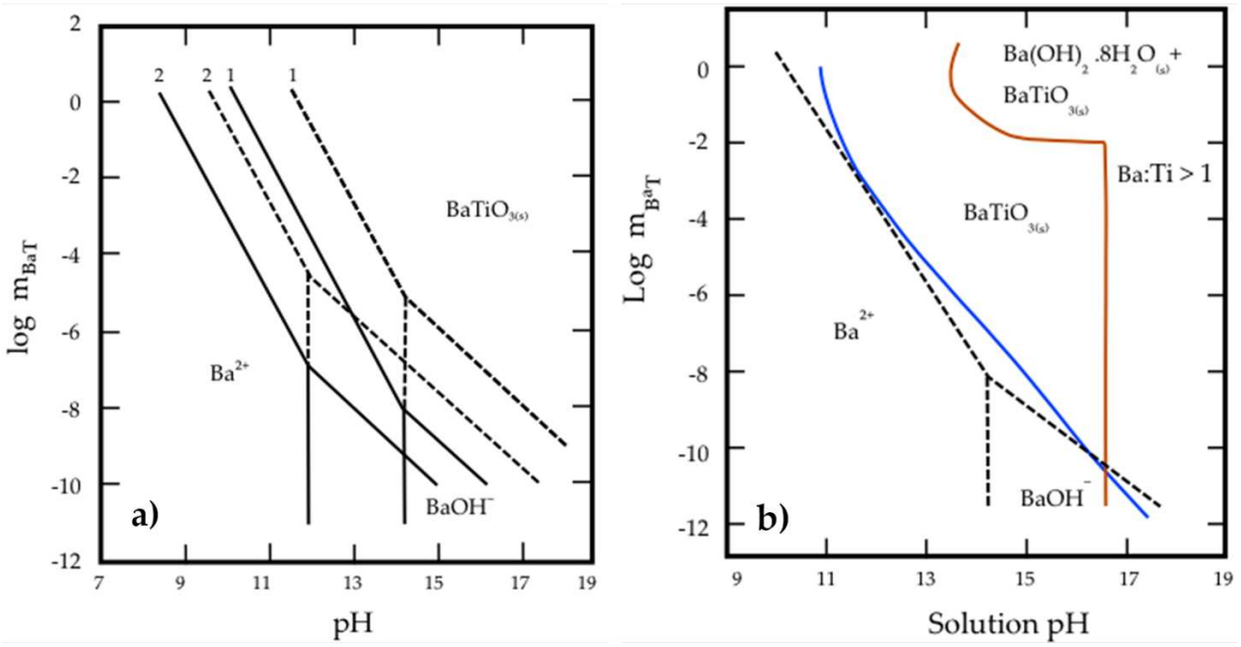

Figure 3. Ba-Ti hydrothermal system stability diagrams calculated (a) using an ideal-solution approximation at 25°C (1) and 90°C (2); the solid and dashed lines denote the results calculated using data from Barin and Naumove, Refs. 15 and 37 in Ref. [40], respectively. And (b) at 25°C using modelled activity coefficients; state standard data were taken from Barin; the dashed line corresponds to the ideal-solution results taken from Lenka and Riman [40].

assumes that all the activity coefficients of the reaction are equal to one (Figure 3a). The variation in the boundaries of stability for the phases contained in the diagram are due to the data set of standard state properties employed to solve the equilibrium of the related species. This particular diagram illustrates the effect of deviation with respect to the ideal-solution boundaries, which were calculated using data for standard state properties from two different sources. Differences on the standard data might markedly shift the boundaries between the stability regions, as is shown in Figure 3a.

Figure 3b gives the results of the complete thermodynamic modelling conducted at 25°C, in which solid lines represent the boundaries of ionic and solid species. For comparison purposes, this diagram includes the boundary (dashed line) calculated with the aid of the ideal-solution approximation. It deserves to be emphasized that significant differences existing between the phase limits calculated using both complete and simplified (ideal solution) models. However, for the ideal-solution model, the bound between ionic species of Ba^{2+} and solid $BaTiO_{3(s)}$, as well as between ionic Ba^{2+}–$BaOH^{+}$, and ionic $BaOH^{+}$–solid $BaTiO_{3(s)}$, are well defined. In contrast, the phase bound determined from the complete model do not follow straight-line functions. The curvature trend is significantly marked at higher concentrations of the aqueous species (Ba (m_{Ba_T}) >10^{-4}). Furthermore, when the solution non-ideality is considered to carry out the modelling, the bounds shifted towards higher pH values. In particular, the phase boundary between Ba^{2+}–$BaOH^{+}$ is shifted by approximately 2 pH units, while that for Ba^{2+}–$BaTiO_{3(s)}$ is changed approximately in 1 pH unit. This behaviour also occurs at higher temperatures between 100 and 200°C.

The stability diagrams do not supply information related to the experimental conditions required to promote the total reaction of the precursors. Assuming that under certain hydrothermal conditions, a total 100% yield of the crystallized reaction product must be produced. Analogous yield diagrams can establish a more practical insight of the hydrothermal processing. This tool has a great potential for establishing the optimum conditions required to achieve a total consumption of the precursors to produce high yields of the desired compound (e.g. ABX_3). Therefore, the yield analysis takes into account the initial input concentration of the precursors, because the equilibrium concentration of species in a saturated solution is of primary concern for the hydrothermal process, because the feedstock must be transformed into a phase-pure product. The yield diagrams consist of sections where a specific amount of the desired product crystallizes involving the total reaction of the precursors. In other words, where the yield product is at least equal to an assumed value, namely 99%, at the stability boundary, the product yield is very small, because only an incipient nucleation of the product occurs at this point. The yield increases as the hydrothermal reaction process is driven beyond the solubility curve into the solid–liquid region. Hence, the product yield is determined by dividing the number of moles of the product by the total number of moles corresponding to the input metal precursors [38, 41–43].

Complex phase diagrams derived by thermodynamic modelling can be developed following the theory and methodology described above. These diagrams include both stability and yield fields and are calculated using the ideal solution and complete models. However, single stability and yield diagrams are portrayed against the solution pH, because this is an independent variable associated with the hydrothermal processing. The concentration of a pH-adjusting solution required to achieve the crystallization of the desired product is not indicated in the diagram. One typical example was derived for the Sr–Zr system, and it is shown in Figure 4. The stability and yield diagrams were calculated for the preparation of $SrZrO_3$ employing strontium hydroxide and zirconium oxide as precursors at 200°C. The diagram was determined at a fixed mixing Sr/Zr ratio of 1 which is plotted as a variable in the y coordinate axis, while the molality of the alkaline (KOH) is portrayed in the x coordinate axis. The solid line in the diagram (Figure 4) indicates the starting point of the crystallization of the $SrZrO_3$ perovskite phase, although $SrZrO_3$ and ZrO_2 might coexist in the field above the solid line as the reaction tends to move closer to the shaded area. The remaining content of ZrO_2 is gradually consumed leading to an increased amount of $SrZrO_3$ produced. The shaded area is related to the optimum conditions, in terms of precursor feedstock: molality of $Sr(OH)_2$ and KOH required to obtain the pure-phase $SrZrO_3$ at a yield above 99% at the treatment temperature of 200°C [40–46].

The thermodynamic model of heterogeneous aqueous ionic liquid is a practical tool to prepare stability and yield diagrams. This powerful tool capable of estimating the effect of various processing conditions is likely towards to conduct the crystallization of smart perovskite ceramic materials in a more cost-effective way. In particular, it is possible to determine adequate conditions such as reaction temperature, pH, input precursor concentration and mixing ratios. The theoretical predictions allow researchers to formulate processing guidelines

http://dx.doi.org/10.5772/61568

for finding optimum synthetic conditions to produce perovskite-type multicomponent compounds.

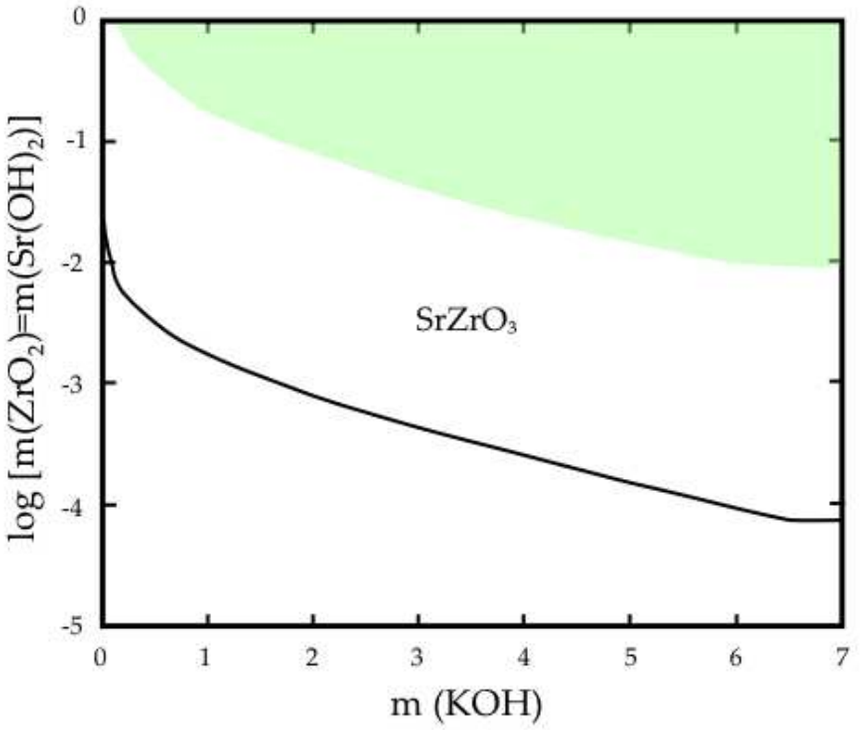

Figure 4. Sr-Zr system phase stability and yield diagram calculated as a function of the solvent content ([KOH]) at 200°C for a precursor mixing ratio Sr/Zr = 1; the precursor source of strontium selected was $Sr(OH)_2$ [40].

2.3. New model based on kinetic precipitation and balance population approaches

2.3.1. Hydrothermal crystallization of ABX_3 based on kinetic and population balance equation

New models based on kinetic and population balance equations have received a tremendous attention. In the past decade, academic and industrial communities have devoted efforts to propose the models and evaluate their functionality to estimate the factors affecting the particle formation in a wide variety of processes. Additionally, the control of particle size of the final particles prepared via hydrothermal crystallization constitutes a potential advantage in comparison with other synthesis processes. Under hydrothermal conditions, the particle size distribution that grows from a solution strongly depends on the nuclei formation rates and subsequent particle growth. At an accelerated nucleation rate, the total number of particles produced is large while their size is relatively small. In a particular hydrothermal reaction system, the rates of nucleation and growth depend on supersaturation. Processing parameters such as precursor feedstock concentrations, temperature, and mixing conditions typically influence the supersaturation. Therefore, the final particle size distribution can be tailored by adjusting the hydrothermal synthesis conditions.

In the past decade, various efforts were conducted in order to present different approaches accounting for the phenomena related with the particle formation of perovskite-structured compounds. Testino et al. have proposed the first meticulous kinetic approach devoted to the formation of $BaTiO_3$ particles, the particle formation is based on a solution precipitation reaction [50–51]. The new model derived for the crystallization of $BaTiO_3$ particles in an aqueous system is based on equations derived from basic nucleation, growth and aggregation fundamentals. This approach does not take into account empirical relationships such as those assumed in the thermodynamic equilibrium models. In contrast, the new model is based on reaction kinetics that correlates a mass balance coupled with a population balance. The population balance concerns the evaluation of some entities in a reaction system, i.e. solid particles or, events that might dictate the particle crystallization behaviour in the hydrothermal system under study. The performance of individual entities depends on variables associated with an appropriate reaction environment; consequently, the population balance equation might be correlated with balance equations that include the environmental variables [50, 52, 53].

The theoretical framework of the kinetic model was conceived by the exhaustive preliminary investigation of the aspects associated with the formation of $BaTiO_3$ particles in an aqueous system [51]. The concentration of barium in the hydrothermal system promotes a variation in the rate of formation of $BaTiO_3$ particles. When the content of Ba^{2+} increases, it decreases the particle size of the crystallized particles, and it also affects the chemical reaction when the temperature is varied; this effect has not been clarified. The model was developed taking into consideration the formation kinetics of perovskite $BaTiO_3$ particles from dilute solutions of $BaCl_2$ and $TiCl_4$ (≤0.1 M) at a value of pH = 14 between 80–90°C. The overall chemical reaction experimentally studied is as follows:

$$BaCl_{2(aq)} + TiCl_{4(aq)} + 6NaOH_{(aq)} \rightarrow BaTiO_{3(s)} + 6NaCl_{(aq)} + 3H_2O_{(l)} \quad (7)$$

where (aq) denotes the hydrolyzed salt in water. The new kinetic model that is applicable to the preparation of different perovskite compounds was correlated with experimental data collected at various alkaline media concentration, temperature and Ba/Ti ratio. The preliminary experimental analysis allowed the researchers to establish the stages and details of the mechanism associated with the nucleation, growth and particle aggregation [50, 51]. In this reaction system, the influence of non-ideality of the aqueous solution, net particle superficial area and thermodynamic properties were not considered.

In agreement with the analysis conducted by Testino et al., chemical reaction 7 occurs in two steps. (i) In the first step, the formation of a titanium hydroxide gel (THG) phase proceeds rapidly. Consequently, (ii) a slower reaction takes place between the THG phase and the Ba^{2+} ions dissolved in solution. When the supersaturation state of solute has reached under the second step of the reaction, the $BaTiO_3$ nuclei spontaneously precipitate. The $BaTiO_3$ crystallization mechanism controls the overall kinetics involved in the hydrothermal synthesis process. The kinetic study of reaction 7 determined that the evolution resembles sigmoidal

http://dx.doi.org/10.5772/61568

curve behaviour, and the particle growth progress observations strongly support a nucleation and growth mechanism occurring in a second step. The global reaction proceeds via a two-step reaction mechanism, which achieves the formation of $BaTiO_3$ via solution precipitation in mild alkaline conditions [50, 51]. Furthermore, the global mechanism also applies to the hydrothermal synthesis of barium titanate at temperatures above 100°C. When the THG suspension obtained by adding an alkaline media (NaOH or KOH) to the aqueous solution containing both $BaCl_2$ and $TiCl_4$ is used as the precursor; the same process is likely to occur when amorphous titanium hydroxide is produced by hydrolyzing a titanium (TiO_2) precursor in a $Ba(OH)_2$ solution. Hence, the global reaction involving both nucleation and growth of the perovskite is given by the following reaction

$$Ti(OH)_{4(aq)} + Ba^{2+}{}_{(aq)} + OH^{-}{}_{(aq)} \rightarrow BaTiO_{3(s)} + 3H_2O_{(l)} \tag{8}$$

It can be assumed that local equilibrium conditions are carried on at the surface of the growing crystal, involving the equilibrium between the Ba^{2+} and $BaOH^{-}$ ionic species, which are correlated by Eq. (9)

$$Ba^{2+}{}_{(aq)} + OH^{-}{}_{(aq)} \rightarrow BaOH^{-}{}_{(aq)} \tag{9}$$

The supersaturation state associated with reaction 8 is interpreted as

$$S = \frac{\left[Ti(OH)_4\right]\left[Ba^{2+}\right]\left[OH^{-}\right]^2}{K_S} \tag{10}$$

The supersaturation solution grade is independent of the solvent species involved in the precipitation reaction; therefore, the equilibrium conditions are kept at the solid/liquid interface for an extended period. The $Ti(OH)_4$ species are provided by the THG precursor phase dissolution. A global mechanism that proceeds in two steps conducts this process. At the first step, the disruption of the polymeric network of $Ti(OH)_4$ takes place by the nucleophilic attack of the OH^- ions occurring at Ti atom positions (denoted as Ti*, in Eq. 11). The second step of reaction comprises the reaction between oxygen ions (O*) produced during the decomposition of $Ti(OH)_4$ with water molecules, restoring the hydroxyl ions. The dissolution rate, which is reversible and rate controlled at the first step, can be expressed by

$$\frac{d\left[Ti_{gel}\right]}{dt} = k_1\left[Ti^*\right]\left[OH^-\right] - k_{-1}\left[O^*\right]\left[Ti(OH)_4\right] \tag{11}$$

where the term $[Ti_{gel}]$ corresponds to the number of moles of titanium contained in the gel precursor in the reacting suspension. Additionally, k_1 and k_{-1} are correlated to the kinetic constants of the direct and reverse process, respectively. When [Ti*] and [O*] are proportional to $[Ti_{gel}]$, Eq. (8) can be rewritten as

$$-\frac{d\left[Ti_{gel}\right]}{dt} = k_1\left[Ti_{gel}\right]\left[OH^-\right]\left\{1-\frac{K}{K_S}\left[Ti\left(OH\right)_4\right]\right\} \tag{12}$$

where k is the rate constant for THG dissolution, and K is the reciprocal of the equilibrium constant overall reaction

$$TiO\left(OH\right)_{2(gel)} + Ba^{2+}{}_{(aq)} + 2OH^-{}_{(aq)} \rightarrow BaTiO_{3(s)} + 2H_2O_{(l)} \tag{13}$$

This general approach likely describes the mechanism applied to the classical hydrothermal process, in which crystalline titanium oxide particles (TiO_2) are suspended in aqueous $Ba(OH)_2$. In this reaction system, the net surface area of the titanium oxide particles affects Ti^{4+} ionic species produced via the dissolution of TiO_2 powder and its dissolution rate.

2.3.2. Mass balance expression

The complete model expression is constituted by two additional terms; the first one takes into account a global mass balance of the ionic species involved in the formation of the ABX_3 single phase. The mathematical expression that involves the mass balance of one of the precursors, i.e. titanium ions, in the hydrothermal system can be written as [50]

$$-\frac{d\left[Ti_{aq}\right]}{dt} = \frac{d\left[Ti_{BT}\right]}{dt} + \frac{d\left[Ti_{gel}\right]}{dt} \tag{14}$$

In this differential equation, the term $[Ti_{aq}]$ indicates the concentration of the aqueous titanium species present in the reaction system, which typically is assigned to the $[Ti(OH)_4]$. Likewise, the content of the precipitated $BaTiO_3$ at a certain time of reaction is $[Ti_{BT}]$. Thus, the first term in Eq. (14) is correlated with the $BaTiO_3$ particle formation rate promoted by nucleation and growth events.

$$\frac{d\left[Ti_{BT}\right]}{dt} = \left\{\hat{B} + \hat{G}\right\} \tag{15}$$

Eq. (16) corresponds to the global equation that combines the nucleation and growth with the dissolution rate of the THG given by Eq. (12). This expression involves the crystallization rate of $BaTiO_3$ by nucleation and growth events coupled with the simultaneous consumption of the THG phase, which is analogous to the yield product term in the thermodynamic models. If the Ba/Ti molar ration in the THG is denoted by R_{gel}, the mass balance can be given by Eq. (17), in which $[Ba_{aq}]$ is the absolute concentration of Ba ions corresponding to the sum of $[Ba^{2+}]$ and $[BaOH^+]$ species.

http://dx.doi.org/10.5772/61568

$$\frac{d\left[Ti_{aq}\right]}{dt} = \mathrm{k}\left[Ti_{gel}\right]\left[OH^{-}\right]\left(1 - \frac{K}{K_S}\left[Ti(OH)_4\right]\right) - \left\{\hat{B} + \hat{G}\right\} \tag{16}$$

$$\frac{d\left[Ba_{aq}\right]}{dt} = R_{gel}\frac{d\left[Ti_{gel}\right]}{dt} - \left\{\hat{B} + \hat{G}\right\} \tag{17}$$

2.3.3. Population balance

The population balance equation (PBE) is related to net particle number continuity. It was the concept introduced to complete the kinetic model. The last term takes into account the evolution of the particle size distribution for a particular cluster of particles subjected to nucleation, growth, coalescence and disruption processes. According to Testino et al. [50], the expression can be given as

$$\frac{\partial n(L,t)}{\partial t} + \frac{\partial}{\partial L}\left[G(L,t)n(L,t)\right] = B\left(n\right) - D\left(n\right) \tag{18}$$

In the PBE equation, $n(L,t)$ corresponds to the density of particles at a particular time t in the particle size range L to L+ dL. While G represents the isotropic growth rate, B and D are the particle rates of genesis and extinction, respectively. The net particles number per unit volume is defined at an infinitesimal period as dN, and the density function is n = dN/dL. Equation 15 is related to the rate of particles accumulation in the range L to L+dL. This range is a function of the particle growth rate and specifically of the speed at which particles of that size are directly created or removed. In order to solve this equation, the kernel aggregation function coupling with the PBE and four particle size distribution moments were considered. Because these are the quantities used to solve PBE problems [50, 52–54].

The new kinetic model derived for $BaTiO_3$ particles is likely applicable to a broad number of perovskite systems, following the methodology described above. In either case, a raw dried titanium hydroxide or Ti-gel formed as an intermediate product are used as a precursor reactant. The nucleation and growth theory for supersaturated solutions correlates the rates of nucleation and growth with some physical parameters such as temperature, the surface tension of the solid phase and diffusion coefficient. In the model, nucleation is considered to occur in two steps, in the initial stage a homogeneous nucleation proceeds in the supersaturated solution. After the conclusion of the preliminary step, a secondary nucleation is then enhanced promoted by the variation of solute saturation in the hydrothermal media. The secondary nucleation controls the creation of new embryos on the surface of $BaTiO_3$ particles, which are already present in the suspension as a result of nucleation and growth events. The secondary nucleation promotes the rapid increase in the $BaTiO_3$ formation rate after the initial period dominated by primary nucleation. Moreover, secondary nucleation leads the polycrystalline nature of the final particles. Diffusion-controlled growth is the process involved in

the coarsening of the elementary crystals that constitute the polycrystalline particles. The new algorithm has a potential for calculating the net number of events (moments) under particular reaction conditions. These events are of particular concern because these define the particles' aspect such as total number, dimension, surface and volume of particles per liquid suspension unit volume. The new model based on a PBE analysis yields an uncertain approximation of the real process, but hinders the introduction of completely empirical relationships between growth rate and supersaturation state.

In general, one limitation of the kinetic model is the use of PBEs considering one internal variable, i.e. the size of the primary crystallites. Consequently, a more meticulous approach proposed takes into account the use of PBEs with at least two internal coordinates, for example, the size of the primary particles and the size of the polycrystalline particles. New approaches might provide a better description by taking into account the interactions between the elementary crystallites affecting the overall precipitation process. However, the application of PBEs with more than one internal coordinate to precipitation problems is still at an early stage of development. Recently, Marchisio has presented a detailed mathematical model involving the precipitation of $BaTiO_3$ in aqueous solution [54]. This particular model is based on a bi-variate population balance equation. The new approach overcomes the limitations considered for a mono-variate population balance equation, namely the crystallite size and particle size. The new improved model (not reported here) shows qualitative results similar to those previously discussed for the mono-variate model. However, quantitatively the modelling results are very different from the predictions obtained with the mono-variate PBE. This complete model can be used to identify new model parameters associated with the mechanism involved in the nucleation, growth and aggregation stages of $BaTiO_3$ hydrothermal synthesis [54].

In the past decades, an increasing interest in the production of submicron powders with uniform particle size distribution (PSD) through solution precipitation methods, including the hydrothermal powder processing, has been the main concern in the chemical engineering field, particularly, the search for the adequate operating conditions for preparing perovskite nanoparticles, similar to those examples described in the following section. However, modelling works on thermodynamics coupled with the kinetic aspects of particle formation and its evolution have also been conducted by various researcher groups in different areas [38–42, 50–54]. The motivations for developing new optimized mathematical models are multiples. Indeed, the mathematical models described in the present review can be used to estimate the hydrothermal conditions for particle formation and the evolution of mechanisms associated with this process. Also, these can be used to set up the optimal operating conditions to prepare a powder with desired characteristics, following a product engineering philosophy. Finally, there is an enormous potential to employ both thermodynamic and kinetic models, by implementing them in computational fluid dynamics models, to scale up the precipitation processes from laboratory to an industrial scale. However, new researchers in the hydrothermal field must bear in mind that some caution must be exercised, when applying the proposed models to diverse perovskite systems, because modelling results might vary depending on the reaction temperature and concentration of precursors. These factors might lead to erroneous conclusions associated with the reaction mechanism operating for a particular reaction system.

http://dx.doi.org/10.5772/61568

Moreover, the models assume that during the nucleation and growth events, the hydrothermal system is perfectly mixed, leading to a precipitation rate being controlled by the chemical reaction kinetics. Although these inferences are acceptable in small laboratory vessels, these might not operate for larger industrial reactors, where mixing problems might frequently rise due to slow and less-efficient agitation systems. The precipitation rate is one of the problems that commonly meets in the scale-up of precipitation processes.

2.4. Hydrothermal processing of perovskite-structured ceramic oxides

According to the literature survey, the synthesis under hydrothermal conditions of different types of perovskite compounds was triggered during the 20th century. Nowadays, this synthesis method constitutes an important tool for materials processing. Because hydrothermal synthesis offers some processing advantages, which enhances the preparation of monodispersed nanoparticles with controlled size and morphology. In the present review, the experimental details for the synthesis of a broad number of perovskites are addressed based on their compositional aspects, namely single substitution in either A or B sites. Some double perovskites and their related solid solutions are also included.

The synthesis of single-phase stoichiometric perovskite ABX_3 has been possible under hydrothermal conditions by the employment of a broad number of atomic elements. Among the elements incorporated at the A site of the perovskite structure are the elements of IA (K, Ag, Na) and IIA (Ca, Sr, Ba) groups of the periodic table. Some bivalent elements (Bi, Pb, Rb) have been incorporated in this site as well. Experimental results demonstrated that trivalent rare earth elements, namely La, Pr, Nd, Sm, Eu, Gd, Tb, Dy, Ho, Er, Tm, Yb, Lu or Y, are able to be located at the A site, while the B site could be occupied by stable transition metals elements (Ti, Fe, Zr, Ta, Nb, Bi, Sn, Co, Ru, Cr and Mn). The next sections of the present review give an account of the main experimental aspects related to the hydrothermal processing of perovskite-structured ceramic oxides. Particular emphasis is placed on the practical aspects associated with the selection of mineralizers and their concentrations, solution pH, choice of precursors, and reaction intervals and temperatures. This review intends to present a more realistic and practical state-of-the-art on the optimization of the synthesis of the major perovskite-structured compounds that have been extensively produced via hydrothermal processing. It deserves emphasis that succeeding on the crystallization of pure single phase perovskite oxides under hydrothermal conditions depends on major functional parameters such as the nature of precursors and mineralizer. The main aspects related to the hydrothermal processing of perovskites are discussed in terms of the type of the site substitution, focusing only on single-phase perovskite oxides. Starting from the synthesis of major A-site-ordered perovskite-structured oxides ($ATiO_3$, $AFeO_3$, $AZrO_3$, etc.) and a few solid solutions, and subsequently proceeding to the synthesis of B-site-ordered perovskites and, finally, to the synthesis of A and/ B-site-ordered perovskite oxides.

2.4.1. Synthesis of A-site-ordered perovskite titanates ($ATiO_3$)

In recent years, much progress has been made in the synthesis of A-site-ordered perovskite titanates ($ATiO_3$; A= Ba, Pb, Ca and Sr; hereafter the compounds containing the latter cations are referred as BT, PT, CT and ST, respectively) under hydrothermal conditions. In the

synthesis of BT particles, various authors have employed different methodologies to prepare powders with perovskite structure under hydrothermal conditions. These methods, in general, enable us to synthesize this kind of perovskite oxides in various aqueous alkaline solutions using various mineralizers. One experimental procedure developed for the synthesis of BT powders use $Ba(OH)_2$ as the precursor of barium and pH adjustment agent, instead of using a strong alkaline mineralizer (KOH or NaOH). The BT particles synthesized at a low temperature of 80°C in a solution with a pH of 8 exhibited a spherical morphology and cubic ABX_3 structure. The chemical reaction promoted under hydrothermal conditions involved the use of chemically modified Ti-peroxo-hydroxide and $Ba(OH)_2$ precursors. The Ti-peroxo-complex precursor was rapidly dissolved in the reaction media ($Ba(OH)_2$), subsequently enhancing the crystallization of BT particles, providing fast and mild powder synthesis conditions [55].

The crystallization of BT particles was found to be carried out with similar morphologic and structural aspects when $BaCl_2$ is employed as a precursor and using NaOH as mineralizer [56]. The optimal concentration of the NaOH mineralizer to conduct the synthesis was 6 M; it allowed to obtain the BT perovskite single phase between the range of 120 and 200°C for reaction periods of 1–4 h. Reaction kinetics influences the crystallization of BT at low temperatures and short reaction times. However, the thermal equilibrium plays a crucial role at elevated temperatures (200°C) and/or prolonged reaction times (4 h) that control the particle crystallization. In other study conducted under similar conditions of synthesis [57], different metal titanates ($ATiO_3$, A= Ba, Sr, Ca), among them BT particles, were also prepared. For this case, the reaction synthesis was developed at highly alkaline conditions with a value of pH > 12. The excess amount of NaOH provided an alkaline environment for the dissolution of TiO_2 and its subsequent reaction to produce BT. They found that the formed Ti-OH complexes reacted at 160°C for 72 h with the Ba^{2+} ions in the solution to form the single-phase BT perovskite oxide.

Other methodologies have been employed to prepare BT powders exhibiting morphologies and particle size, using KOH as a mineralizer. Recently, nanocrystalline particles with a cubic shape of BT were prepared using organic compounds; these promoted the control of the particle size during the crystallization step. In this case, the hydrothermal media consisted in a KOH solution prepared with 11 mmol of reagent (2.2 M) [58]. In contrast, different perovskite-structured BT oxides were prepared from altered titanium isopropoxide and barium acetate salts controlling the pH of the suspension adding a 2.0 M KOH solution [59]. Under these conditions, phase-pure perovskite BT powders were successfully synthetized at 150°C for 18 h in an extremely alkaline feedstock media. The pH of the suspension was 13; it was concluded from this study that a strong alkaline solvent is necessary for the production of pure-phase perovskites under hydrothermal conditions. In a subsequent study, the effect of varying the molar [KOH]/[Ti-isopropoxide] ratio during the reaction synthesis was investigated. The principal aim was to determine the impact of this processing factor in the crystallinity and particle size of the BT particles [60]. In this particular reaction system, the nucleation and growth processes are affected by the electric charge micelles produced on the surface of the BT particles during the hydrothermal process. The increment in OH^- concentration caused by dissolution of KOH in the reaction medium improves the tendency to BT particles separation,

http://dx.doi.org/10.5772/61568

because the generation of electrostatic repulsion forces acting in-between negatively charged surfaces hinders the formation of BT agglomerates [60].

Later on, Xiao and co-workers [61] developed another methodology to synthesize BT powders with spherical morphology. In this approach was involved the usage of a surfactant agent such as ethylene glycol in a 1 M KOH solution. After 200°C for 12 h, the experimental results showed evidence of the formation reaction by-product, namely traces of $BaCO_3$, which was removed by acid washing. The synthesis of BT with dendritic shapes without any surfactants was conducted using KOH solutions with various concentrations of 0.1, 0.3, 0.7 and 1 M, keeping other reaction conditions unchanged (200°C, 12 h). It was found that the KOH concentration was a crucial parameter that enhances the formation of the BT dendrites [62]. When the concentration of KOH increased, the particle morphology changed from dendritic to a sphere-like shape. This phenomenon was explained based on the fact that dendritic growth tends to take place as the system is driven farther away from equilibrium. Therefore, when low KOH concentrations were used as solvent, the alkalinity of the media did not allow the system to reach the equilibrium conditions. This fact promoted the formation of the BT dendrites rather that the sphere-shaped particles [62].

Under microwave-hydrothermal conditions, the synthesis of BT powders was accelerated in comparison with conventional hydrothermal synthesis. Zhu et al. [63] satisfactorily synthesized perovskite BT nanowires in different reaction media using pure water and mixtures of water–ethylene glycol solutions. The pH value of the resultant mixture was adjusted to 14.0 adding 1.1217 M of KOH before the hydrothermal treatment. A substantial reduction of the reaction time was achieved using a highly concentrated alkaline solvent, allowing the synthesis of pure-phase BT particles to proceed for 50 min at 150°C. The alkalinity of the hydrothermal media had a significant influence on the crystal structure of the single-phase BT and affected the morphology of the BT powders produced by hydrothermal-microwave-assisted treatments [64]. The BT nanoparticles prepared under microwave-assisted sol-hydrothermal conditions exhibited a varied morphology accounting from elongated particles to a ring-like shape. The differences in particle morphology occurred by changing the KOH concentration from 0.25 to 5 M. The reaction involves the metal hydrous complex gel formation that is promoted by dissolution of the precursors, and the subsequent recrystallization when the solvent reaches the supersaturated state. The nuclei were rapidly transformed into BT nanoparticles because of the high pH and high reaction temperature. The nanoparticles that resulted from the high saturation of the reaction solution dissolved in the solution forming additional nuclei avoiding a marked particle growth [64].

On the other hand, the synthesis of PT particles has been extensively investigated under different hydrothermal conditions. Ohara et al. [65] conducted one of the pioneering research works for preparing PT perovskites. The optimum conditions for preparing pure PT single-phase fine fibers were 150°C for variable reaction times (24 to 72 h). The PT fibers were produced selecting a molar Pb/Ti ratio = 1, and Ti ions were supplied by adding potassium titanate $2K_2O \cdot 11TiO_2 \cdot 3H_2O$ as the precursor material. These authors also demonstrate that the hydrothermal technique provides the possibility to prepare PT fine powders with spherical morphology. The morphological particle transition from fibrous to spherical was obtained via

an ion-exchange reaction between Pb^{2+} ions and K^+ ions. This phenomenon occurs under hydrothermal conditions at high pH, 150°C, and pressure (0.4–0.5 MPa). The formation of the PT phase requires a Pb^{2+} concentration higher than that of K^+ in the system. Likewise, by employing, additionally to the KOH concentration, other mineralizer salts, such as $NaNO_3$, KNO_3 and $LiNO_3$ in the reaction media, it was possible to obtain tetragonal perovskite PT nanosheets [66]. The synthesis of pure perovskite PT with tetragonal structure was carried out in a suspension with KOH and $NaNO_3$ concentrations of 1 and 4 M, respectively. According to these studies, it was found that the PT synthesis preferentially occurred under stoichiometric equilibrium conditions.

Miscellaneous research works were carried out to investigate the favourable conditions for synthesizing CT and single-phase RCT doped with rare earth elements (R = Eu) perovskites. These were compounds prepared using the soft chemical process microwave-hydrothermal method without the usage of organic surfactants [67, 68]. The synthesis of pure-phase orthorhombic CT and RCT was successfully carried out in a reaction media with a pH value of 14 using KOH as the mineralizer. The presence of the alkaline solution promoted the co-precipitation of a complex hydroxide constituted by the $TiO(OH)_2$-$Ca(OH)_2$-$Eu(OH)_3$ during the early stage of the reaction. During the formation of either CT or RCT compounds, the direct rotational water excitation that is achieved by microwave radiation produced the release of uncoupling OH^- groups from the complex hydroxide. Consequently, calcium and $Ti(OH)_4$ clusters rapidly interact themselves in the aqueous media as a result of the preliminary OH removal process. Therefore, at a pH ≥ 9, the heating promoted by microwave radiation achieved the CT and RCT nucleation, respectively. Under these conditions, the crystallization kinetics of both perovskite-structured compounds was accelerated one to two orders of magnitude. Thus, it was presumed that the diffusion of calcium and titanium clusters is higher under hydrothermal conditions than at ambient pressure and temperature. This phenomenon was explained to proceed by effective particle collisions producing irreversible oriented attachments that offer favourable thermodynamic and kinetics conditions for the crystallization of CT and RCT, in addition to the particle shape control.

Regarding the synthesis of ST perovskite, it was conducted in KOH solutions with concentrations as low as 0.1 M. The ST nuclei precipitated incorporating mild concentrated $Sr(OH)_2$ solutions in the hydrothermal system, and many Sr^{2+} ions remained in solution after the crystallization process. However, a large amount of $Sr(OH)_2$ remained when the KOH concentration was increased up to 1 M, and the mass transport rate of ions that feed the growing crystals was accelerated. Therefore, a variety of crystal surfaces have the opportunity to grow due to the relatively larger rate of ionic mass transport, which allowed the formation of cubic-like-shaped ST aggregated crystals [69]. Figure 5 gives the typical micrographs of ST perovskite powders hydrothermally prepared at 250°C for various reaction intervals [70]. Finally, the hydrothermal synthesis of some solid solutions was satisfactorily carried out under conditions similar to those mentioned above. Wei et al. [71] prepared pure-phase $Pb_{0.70}La_{0.30}TiO_3$ fine powders with cubic structure by employing co-precipitated Pb-La-Ti-OH_X hydroxide and KOH solutions with different concentrations of 2, 4 and 6 M at 220°C for 36 h. Additionally, in another set of experiments, the synthesis of $Bi_{0.5}Na_{0.5}TiO_3$ (BNT) was found to occur in highly

http://dx.doi.org/10.5772/61568

concentrated alkaline hydrothermal media of 12 M NaOH. This concentration is the minimum required to achieve the crystallization of single-phase BNT particles at a lower temperature as 160°C for a short time of 3 h [72].

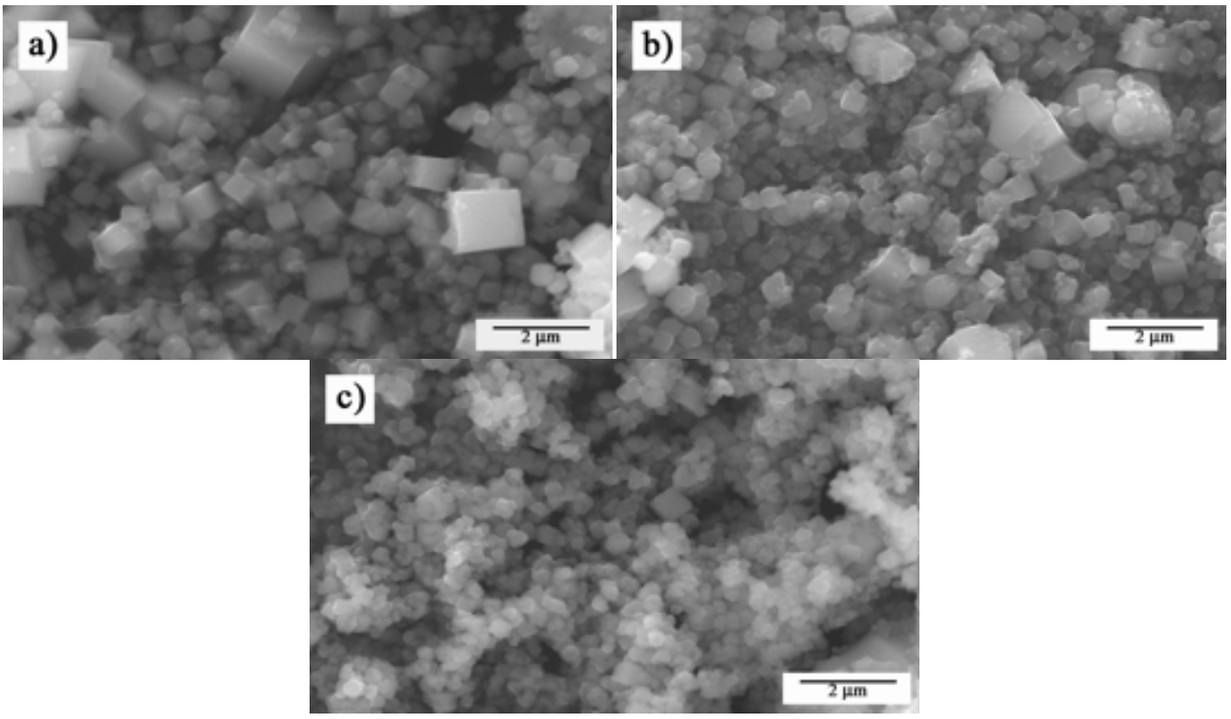

Figure 5. SEM Micrographs of ST perovskite obtained under hydrothermal conditions at 250°C in a KOH solution (5 M) after (a) 0.08, (b) 1 and (c) 24 h [70].

2.4.2. Synthesis of ferrite type perovskite ($AFeO_3$)

Recently, the synthesis of multiferroic materials such as perovskite BF has received intensive scientific attention because of its magnetic and ferroelectric properties. A particular interest has been paid for preparing submicron BF powders with the assistance of NaOH mineralizer at lower temperatures (150–190 °C). The reactant reagents used were $Bi(NO_3)_3$ and $FeCl_3$ [73]. In this particular case, the crystallization of the perovskite-structured BF powders with hexagonal structure occurred in low concentrated NaOH solutions, 0.03–0.12 M, at 170°C for 16 h. The BT perovskite phase crystallization and particle morphology were affected by processing parameters such as solvent solution concentration, reaction temperature and time. The parameter that strongly affects the crystallization step was the concentration of the solvent solution of NaOH. At a low concentration of NaOH media, below 0.03 M, a large number of water molecules and a few $[Na(H_2O)_n)]^+$ cations coexist in the aqueous media. The presence of these species reduces the rate of the crystallization of the amorphous precursor colloid phase that contains Bi_{3+} and Fe_{3+} ions. Therefore, the principal mechanism associated with the nucleation and growth stages involves an in-situ gel transformation process. The amorphous colloid gel transformation occurs under early and intermediate step of the crystallization

process. This fact is likely to proceed when water molecules are removed from the structural gel network enabling the nucleation of small embryos. The gradual increase of temperature and solvent concentration promotes the presence of a few number molecules of water together with a large number of $[Na(H_2O)_n]_+$ cations. These species accelerate the dissolution rate of the amorphous precursor, enhancing a rapid dissolution–recrystallization process. Once the solution was supersaturated, nucleation and crystallization took place faster in the saturated solvent solution [73].

The control of the BF particle morphology can be achieved under hydrothermal conditions. BF pure-phase microplates with rhombohedral structure were preferentially synthesized at 200°C for 8 h, using $C_6H_{10}BiNO_8$ as a Bi precursor reactant and particle surface modifier [74]. The synthesis was carried out in a suspension obtained adding a 0.4 M KOH solution. The formation of the perovskite BF rhombohedral structure was achieved by a self-assembly process coupled with coarsening stage promoted by the Ostwald ripening growth mechanism. A process comprising different steps explained the production of the BF pure phase. The nuclei are generated in the supersaturated solution yielding the growth of $Bi_{25}FeO_{40}$ spherical-shaped nanoparticles during the first of the reaction. Then, these spherical nanoparticles underwent an oriented aggregation due to the preferential 2D plane growth that transformed the spheres into BF nanosheet particles. The adsorption of the $C_6H_{10}BiNO_8$ might modify the formation mechanism because this organic compound prevents the contact between the facets on which the adsorption selectively occurred. Finally, the gradual particle growth produced the formation of microplates that occurred via a repeated dissolution–crystallization mechanism.

The hydrothermal synthesis of BF has also been performed using highly concentrated alkaline solutions. A study directed towards to produce large-scale polyhedral BF particles was conducted at 200°C for 12 h using KOH solutions with concentrations varying between 1 to 9 M [75]. The total OH^- ions concentration affected the agglomeration rate and the particle morphology control. The variation of KOH solvent concentration, reaction time, heating and cooling rates were considered to determine the particle morphology changes of the BF submicron particles. The formation of the large-scale BF polyhedron occurred due to the selective particle aggregation that was promoted via the dissolution–crystallization mechanism. When the concentration of solute reached the critical supersaturation required to enhance the embryo nucleation, the hydrothermal conditions simultaneously preceded the nucleation and growth of small crystallites and subsequently these BT particles nanoparticles underwent a marked agglomeration. Likewise, at low KOH concentrations, the solvent is not capable of controlling the particle surface energy, in consequence the BF nanoparticles underwent a marked agglomeration forming isotropic sphere aggregates. However, when saturated KOH solutions were used, the KOH favoured the control of the particle surface energy, and the particle growth was dominated via an oriented attachment process, which conducted the formation of euhedral-shaped particles.

In a different set of hydrothermal experiments, the crystallization of BF particles was obtained 220°C for 6 h in a 4 M KOH solution [76]. In contrast, above a critical KOH concentration, the formation of secondary impurity phases was favoured. Likewise, the formation of pure BF was strongly dependent on the KOH solvent concentration. During the progress of the hydrother-

http://dx.doi.org/10.5772/61568

mal treatment, the hydroxides species of $Bi(OH)_3$ and $Fe(OH)_3$ were further dissolved in the solvent (KOH), and those reacted at high temperatures and pressures. The solvent saturation provoked the precipitation of the chemically stable ceramic oxide particles. The particle coarsening continues gradually as far as the hydrothermal system maintains a steady supersaturated state. Therefore, the dissolution and crystallization process progressed in the supersaturated fluid because the system tends to reach stability by itself. It was argued that the dissociation of bismuth and iron hydroxide coupled with the formation of complexes ionic could hinder the growth of BF crystallites and limit the size of BF particles to the submicron range. Other studies related to the synthesis of BF where performed for Jiang et al. [77]. These authors carried out the hydrothermal synthesis of BF single crystals using hydrate sodium bismuth oxide ($NaBiO_3$ nH_2O), $Fe(NO_3)_3$ and KOH. Rhombohedral-structured perovskite was obtained with a K/Bi molar ratio of 180 at 180°C for 7 days. However, chemical analyses showed that the molar ratio of the reaction product Bi:K:Fe was equal to 0.96:0.03:1.00, also detecting a small amount of potassium. From these results, the chemical composition of BF large crystals could be deduced to be $Bi_{0.96}K_{0.03}FeO_3$. Taking into account the starting compound with Bi^{5+}, the charge balance of this compound may be obtained by the presence of a mixed valence Bi atoms, resulting in the formation of a compound of $Bi^{3+}_{0.915}Bi^{5+}_{0.045}K^{+}_{0.03}Fe^{3+}O_3$.

On the other hand, the synthesis of BF particles has been possible to carry out at low temperatures with the aid of polymers and surfactants such as PVA [78]. The nanoparticles with spherical morphology have an average diameter of about 10 nm; these were satisfactorily synthesized at 160°C for 9 h in a suspension containing 15 ml of PVA. In a second run of experiments a KOH solution without surfactant addition was used as solvent. The pH value of the residual solution after the hydrothermal treatment was 8; this value is high because a highly concentrated KOH (12 M) was added prior the treatment. The polymer decreased the growing speed of BF nuclei enhancing the formation of nanoparticles. In accordance with the former results, the authors concluded that the polymer addition limited the crystal growth, and the crystal growth rate must be slower than the rate associated with the BF embryo nucleation [78]. Furthermore, experimental works were conducted to study the particle morphology control of BF by using $BiCl_3$, $FeCl_3$ and KOH [79]. In the method investigated, the concentration of the KOH solutions varied in the range of 0.2 to 0.7 M, and the hydrothermal synthesis was carried out at standard conditions at 180°C for 24 h. The control of particle morphology was investigated employing organic surfactant with a concentration of 0.2 M (PEG, EDTA, CTAB and PVP). The surfactant was added to the KOH solution prior the mixing of the Bi and Fe precursors. The usage of concentrated KOH solutions produced a marked agglomeration of particles, which gradually dispersed at long reaction intervals. The morphology of the particles also gradually becomes more regular and homogeneous. A mechanism based on the presence of electrostatic charge micelles is likely to promote the dispersion and morphology control of the BF particles. The micelles formed when a large amount of OH^- cover the surface of the growing BF particles, generates a network of negatively charged nuclei. The repulsive forces between the nuclei are strong, and after the repulsive force reaches its maximum level, it conduces to particle isolation. Therefore, the decrease of KOH concentration in the hydrothermal system provokes the loss of the repulsive force that causes the marked particle aggregation [78].

Other studies focusing on the synthesis of BF particles via hydrothermal processing were performed in reaction media containing organic solvents, namely ethanol or acetone. Recently, Chen et al. [80–81] studied the crystallization of BF particles at low temperature using these organic solvents, which were mixed with the 4 M KOH solution. Well-crystallized pure rhombohedral structure BF nanoparticles were prepared at 120°C for 16 h with an ethanol/water ratio of 4:3 [80]. In this typical hydrothermal process, the ratio ethanol/water had a significant role in the formation of pure BF. Later on, BF powders were synthesized with the aid of acetone, using bismuth and iron nitrates as reactants and a KOH solution concentration of 7 M. The study was directed towards to investigate the effect of solvent (KOH/acetone) on the chemical stability of the reaction product. The BF powders were prepared by using acetone as a solvent to dissolve the nitrate. Then, the suspension was hydrothermally treated at 130°C for 12 h; these conditions yield to the formation of nanometric-sized cubic-shaped particles of BF [81]. The preferential formation of the BF powders occurring at very low temperature was explained as follows: (1) the metal elements have different electronegativities, 2.02 for Bi and 1.83 for Fe. This difference might cause a variation in the hydrolysis rates of the salts employed; in practice bismuth salts hydrolyze more easily in water in comparison with the iron salt. The hydrolysis of $Bi(NO_3)_3$ rapidly occurred resulting in the subsequent formation of a white insoluble precipitate as it is expressed by chemical reaction 19.

$$Bi\left(NO_3\right)_{3(aq)} + H_2O_{(aq)} \rightarrow BiONO_{3(s)} + 2HNO_{3(aq)} \tag{19}$$

The usage of acetone as solvent might limit the hydrolysis of bismuth salt, keeping the element as ionic species with their different electronegativities. Therefore, it might reduce the energy required for successful dissolution and precipitation to form the BF phase during the hydrothermal process. Because the presence of insoluble $BiONO_3$ does not proceed in the system, in contrast only $Bi(OH)_3$ and $Fe(OH)_3$ hydroxides (acting as precursors) precipitates. (2) The increase of the vapour pressure in the vessels is likely to proceed due to the evaporation temperature of acetone, which is 56.05°C. The excess of pressure derived from the evaporation of acetone might accelerate the processes of dissolution and crystallization, and, finally, it leads to the formation of pure BF powders at low temperature. (3) A surface tension phenomena produced by the liquid phase can control the reaction mechanism associated with the crystallization of BF particles. The mechanism is likely to proceed due to the surface tension differences existing between acetone, water and absolute ethanol (23.02, 77.82 and 22.39 m/Nm, respectively). Under hydrothermal conditions, if the surface tension of solvent is high leading to hydroxide precipitation, these intermediate reaction products subsequently are likely to undergo into agglomeration. Therefore, longer reaction intervals are required to transform the hydroxides into BF via a dehydration process. When a small volume of an organic compound is mixed with water, i.e. acetone, the surface tension of the solution must decrease, leading to a rapid hydroxide precipitation achieved by the surrounded solvent. The precipitates had a homogeneous dispersion and were easily dehydrated to form BF powders. Another statement proposed to explain the BF synthesis indicates that, (4) the dielectric constant "ε" of the solvent could be lowered due to the organic solvent addition in water to form the hydrothermal media.

http://dx.doi.org/10.5772/61568

Thereby, the reduction on "ε" causes the decrease of the BF solubility, promoting a high-saturation Bi and Fe in the solvent media. When this state is reached, it provides the optimum conditions for a rapid nucleation of the BF phase. The presence of acetone accelerates the dissolution of the reactants, enabling the crystallization to occur in the supersaturated fluid, finally leading to the achievement of pure-phase BF powders at a very low temperature [81].

The synthesis of a perovskite composite with a composition of 0.5BF-0.5BT was satisfactorily obtained at 200°C employing a KOH concentration of 4 M for 6 h [82]. The crystallization of perovskite 0.5BF-0.5BT is achieved by a "dissolution and crystallization process"; this theory has been widely applied to explain the hydrothermal reaction pathways. The relevant chemical reactions that occur during the synthesis that are correlated with the crystallization of BF-BT are as follows (reactions 20 to 24):

$$2Bi\left(NO_3\right)_{3(aq)} + 6KOH_{(aq)} = Bi_2O_{3(s)} + 6K^+ + 6NO^-_3 + 3H_2O_{(l)} \tag{20}$$

$$Fe\left(NO_3\right)_3 + 3KOH = Fe\left(OH\right)_3 + 3K^+ + 3NO^-_3 \tag{21}$$

$$TiCl_4 + H_2O = TiOCl_2 + 2HCl \tag{22}$$

$$TiOCl_2 + 2HCl + 4KOH = Ti\left(OH\right)_{4(aq)} + 4K^+ + 4Cl^- + H_2O_{(l)} \tag{23}$$

$$Ti\left(OH\right)_4 + 2OH^- = \left[Ti\left(OH\right)_6\right]^{2-} \tag{24}$$

When the hydrothermal synthesis takes place, several reactions occurred between the reactants of bismuth oxide, iron III hydroxide, barium hydroxide and titanium hydroxide. To produce the desired crystalline phases following the chemical reactions 21 and 22 must occur in the hydrothermal system at particular conditions of temperature, time and pressure. Additionally, the results demonstrated that the reaction temperature and the KOH concentration must be optimized to limit the presence of reaction by-products. Under these conditions, the formation of perovskite 0.5BF-0.5BT is likely to be conducted following a single-step reaction.

$$Bi_2O_3 + 2Fe\left(OH\right)_3 = 2BiFeO_3 + 3H_2O \tag{25}$$

$$Ba^{2+} + \left[Ti\left(OH\right)_6\right]^{2-} = BaTiO_3 + 3H_2O \tag{26}$$

A reduced number of researchers have carried out the synthesis of RF (R= rare earth elements group or Y) under hydrothermal conditions using rare-earth nitrates as precursor feedstock. The hydrothermal synthesis of RF particles was conducted in highly concentrated alkaline solvents between 2 and 44 M for 48 h, whereas the reaction temperature required to promote the crystallization of the single ABX_3 phase varied between the range of 230 up to 240°C [83–85]. The formation mechanism of the RF crystals was associated with a precipitation process promoted by the precursor dissolution and nucleation processes. The role of alkalinity was a crucial parameter to control the dissolution, nucleation and growth processes because the chemical reagent precursors are chemically stable even in strong alkaline solvents such as NaOH or KOH.

Similar to the BT powders, the microwave hydrothermal synthesis has been used to synthesize perovskite BF to achieve fast crystallization kinetics and control microstructural aspects of the particles. The hydrothermal crystallization process assisted by microwave radiation accomplishes the formation of BF single phase with rhombohedral structure, for very short reaction intervals of 1 h. The precursor selected to perform this reaction were the reagent-grade salts of bismuth ($Bi(NO_3)_3$) and iron ($FeCl_3$, $Fe(NO_3)_3$). The synthesis process can occur at temperatures in the range of 150–200°C in KOH solutions with concentrations varying between 0.05 and 4 M [86, 87]. Experimental results indicate that crystallization of pure-phase BF powders is possible to take place at 200°C for 1 h with a KOH concentration of 0.05 M, due to the fast heating supplied by the microwave radiation with the aid of the precursor feedstock selected [86]. One point that deserves emphasize is related to the abnormal growth of the BF particles; this causes marked agglomeration of the BT particle. This fact is proposed to be the primary reason for the occurrence of a change in the crystal structure because a high OH^- concentration favours the nucleation process. Moreover, Wang et al. [88] studied the synthesis of BF by using a polyanion, poly(methyl vinil ether-alt-maleic acid) (PMVEMA), KOH and Na_2CO_3 solutions with concentrations of 1 and 8 M, respectively. The BF pure phase was synthesized under the same conditions determined elsewhere [87], and a simple ultrasonic purification method was developed to obtain the pure phase. In particular, PMVEMA was selected because it contains a large number of –COOH groups that operate as anions, which avoid bringing other metal ions. Additionally, the presence of these ions also can control the concentration change of metal ions such as Na^+ and K^+ in the hydrothermal reaction system [88].

2.4.3. Synthesis of zirconite-type perovskite ($AZrO_3$)

Another oxide compound of interest due to its potential applications is the perovskite BZ. Continuous synthesis technologies that allowed the researchers to produce tens of grams of powder products per production hour are devoted to developing at an industrial level. The perovskite BZ phase has been obtained by a continuous hydrothermal synthesis proceeding in a single step under supercritical conditions [89, 90]. The cubic BZ pure-phase particles have been produced at higher temperatures around 450–500°C using NaOH as the solvent media. A high temperature is necessary to complete the release of OH– ions coupled with the neutralization of protons, because at severe supercritical conditions the reaction vessel can suffer a rapid acidic corrosion. The reactions that occur in the autoclave vessel are described

http://dx.doi.org/10.5772/61568

by chemical reactions 27 to 29. Before the occurrence of these reactions, the dissolution of the precursors must take place, due to rapid ionic mobility enhanced by the dielectric constant of the solvent "ε":

$$Ba\left(NO_3\right)_2 \rightarrow Ba^{2+} + 2NO_3^- \quad (27)$$

$$NaOH \rightarrow Na^+ + OH^- \quad (28)$$

$$ZrO\left(NO_3\right)_2 \rightarrow ZrO^{2+} + 2NO_3 \quad (29)$$

The crystallization goes further under supercritical when the precursors are mixed because of the high ionic mobility in the solvent phase due to the low dielectric constant. The reaction that occurs is described as follows:

$$ZrO^{2+} + Ba^{2+} + 2OH^- \rightarrow BaZrO_{3(s)} + 2H^+ \quad (30)$$

In contrast, the possibility of preparing BZ powders with cubic structure was investigated under hydrothermal conditions at 130°C for 24 h. In these experiments, the adjustment of hydrothermal media feedstock to a value of 13 occurs by adding a KOH solution with a concentration of 0.5 M [91]. Furthermore, the formation of RBZ perovskite solid solutions with cubic structure required a minimum reaction temperature of 200°C for 24 h. The reaction was conducted using a highly concentrated KOH of 16 M as a solvent; the strong alkaline solutions rapidly dissolved the reactant precursor [92]. The morphology of the RBZ particles obtained under the severe alkaline hydrothermal conditions resembled hollow nanospheres. However, the particle sizes were simply controlled varying the Rb content in the precursor and keeping the KOH concentration constant. It was confirmed that adjusting the KOH concentration would change the inter-particle force, varying the size of the aggregates.

2.4.4. Synthesis of lanthanum chromites and manganites-type perovskites and their solid solutions ($LaCrO_3$, $LaMnO_3$)

In recent years, much work has been conducted for synthesizing perovskite-type $LaCrO_3$ and $LaMnO_3$ (LC and LM) under mild hydrothermal conditions. There are several reports on the preparation of nanoparticles under hydrothermal conditions. Zheng et al. [93] studied the effect of solvent alkalinity by employing KOH with concentrations between 2 and 16 M. Another parameter evaluated in this work was the molar ratio of KOH/Cr = 10–80, the hydrothermal treatments were carried out at a 260°C for a fixed time of 7 days. These authors found that a highly concentrated alkaline solvent is required when the selected B-cation has an amphoteric behaviour, as it is the particular case of Cr^{3+}. Therefore, the formation of pure LC required ≥8 M of KOH in the reaction medium.

A series of solid solutions based on the perovskite-type structure has been hydrothermally prepared. The synthesis of $La_{1-x}Sr_xCrO_3$ (LSC) with orthorhombic structure has been carried out using different reaction media to prepare in a preliminary stage the co-precipitated gel precursor. Perovskite LSC powders were produced using Triton non-ionic surfactant and NH_4OH as co-precipitation medium; the pH of the starting aqueous media was 8. The reaction rate associated with this process was affected by the common ion effect caused by the metal precursor as well as by the steric barrier due to the presence of the surfactant micelles [94]. Also, the synthesis of LSC fine powders in a media with a NaOH concentration of 0.5 M was achieved by the dissolution–crystallization mechanism. The solvent even at the concentration selected enhances a homogeneous nucleation leading to the formation of dispersed particles. The hydrothermal solvent chemically reacts with the solid species incorporated into the vessel, producing the dissolution of all solids and the ionic saturation of the aqueous solvent media. In consequence, a spontaneous precipitation of LC and LSC powders occurs [95]. The synthesis of these powders also proceeded in a reaction medium of KOH solution. In this procedure, the KOH solution was mixed in two steps. Firstly, KOH was mixed with $CrCl_3$ and to produce $Cr(OH)_3$, while in the second step KOH was used to adjust the alkalinity of the reaction medium after the sources of Sr and La were added. Moreover, a higher alkalinity is necessary for the preparation of LSC because Cr^{3+} behaves as an amphoteric element. In fact, the optimum alkalinity range that promotes the crystallization of LSC solid solutions is from 5 up to 8 M [96]. A similar reaction pathway was determined for the synthesis of rare-earth and yttrium orthochromite perovskites. Because when a rare earth element partially substitutes one of the major constituents in the perovskite structure, it provokes that a concentrated alkaline solution must be used as a precursor solvent (i.e. 10–12 M KOH) [97].

Several types of lanthanum manganite solid solutions have been synthesized under hydrothermal conditions. The synthesis of LBM nanowires ($La_{0.5}Ba_{0.5}MnO_3$) with cubic perovskite structure was produced at 270°C for 25 h with a net [OH–] = 10 M; using $La(NO_3)_3$, $Ba(OH)_2$, $KMnO_4$ and $MnCl_4$ as precursors [98]. Likewise, at the similar conditions of synthesis of LCM ($La_{0.5}Ca_{0.5}MnO_3$) solid solution with orthorhombic structure was produced. The reaction associated with the hydrothermal processing investigated is given as follows [99].

$$\begin{aligned} &3KMnO_{4(aq)} + 7MnCl_{2(aq)} + 5La\left(NO_3\right)_{3(aq)} + 5Ca\left(NO_3\right)_{2(aq)} + 36KOH_{(aq)} \rightarrow \\ &10La_{0.5}Ca_{0.5}MnO_{3(s)} + 18\,H_2O_{(aq)} + 25KNO_{3(aq)} + 14KCl_{(aq)} \end{aligned} \tag{31}$$

Recently, perovskite LSM ($La_{1-x}Sr_xMnO_{3+\delta}$) were obtained at 150°C for 20 h by adjusting the suspension (hydrothermal media) pH to a value of 9 with an ammonia solution. Based on the results of preliminary runs, a systematic study was conducted aiming to obtain the desired chemical compositions of solid solutions of manganite [100]. A mechanism of dendrite nucleation leads to the synthesis of this particular perovskite compound. This fact was established based on the crystalline phase evolution analyses of the reaction product produced after each treatment, which was conducted in a hydrothermal media of 4 M NaOH. It was found that the SLM solid solution with hexagonal perovskite structure and with particle

http://dx.doi.org/10.5772/61568

morphology of hexagonal platelets was formed at temperatures below 220°C. In contrast, the mechanism of embryo nucleation differs when the reaction temperature was 240°C. At this temperature, the LSM particles were formed via the epitaxial nucleation; this mechanism acts preferentially at the edges of the hexagonal platelet. In consequence, the growth of "tree-like" LCM dendrites is promoted under the hydrothermal conditions investigated [101]. In recent years, Spooren et al. [102] studied the synthesis of LCM, LSM and LBM solid solutions using a KOH reaction media; the use of other solvents was also investigated. However, in all the new solvents tested, the formation of reaction by-products was not avoided. The hydrothermal synthesis of LBM, LSM and LCM were achieved in the KOH solvent solution for different molar compositional ratios of:

Mn^{2+}:MnO_4^{2-}:Ba^{2+}:La^{3+}:KOH:H_2O equivalent to 7:3:5:5:1250:3256 at 240°C for 24 h.

Mn^{2+}:MnO_4^{2-}:Sr^{2+} :La^{3+}:KOH:H_2O equivalent to 7:3:5:5:1250:3256 at 240°C for 24 h.

Mn^{2+}:MnO_4^{2-}:Ca^{2+}:La^{3+}:KOH:H_2O equivalent to 7:3:5:5:1250:3256 at 270°C for 24 h.

At present, there are several authors interested in the study of perovskite solid solutions. [103–104]. The investigations were directed towards to develop a simple route of synthesis for LCSM ($La_{1-x}Ca_xSr_xMnO_3$) solid solutions with orthorhombic structure and cuboidal morphology. The synthesis was conducted at 240°C for 72 h. The preparation of perovskite LAM ($La_{1-x}Ag_xMnO_3$) occurred employing the conventional hydrothermal and microwave-assisted hydrothermal method with a reaction media saturated with NH_4OH solution to adjust the solution pH at 8.5 [105]. Furthermore, orthorhombic perovskite manganates YCM ($YMnO_3$, and $Y_{1-x}Ca_xMnO_3$, x = 0.07, 0.55, 0.65) were prepared in one step by a mild hydrothermal synthesis. The optimum concentration of the alkaline solvent media employed to conduct the hydrothermal crystallization 23 M to stabilize the single phase of YCM [106]. The pH of the solvent solution is a critical parameter to achieve the crystallization of PSM and NSM manganites. The adequate KOH molar concentration that favours reaching the equilibrium between the dissolution crystallization events are between 5.0 and 10 M. Therefore, the synthesis of solid solutions PSM ($Pr_{0.5}Sr_{0.5}MnO_3$), NSM ($Nd_{0.5}Sr_{0.5}MnO_3$) and alkali-earth manganese oxides such as 4H-$SrMnO_3$ and 2H-$BaMnO_3$ were conducted using KOH with concentrations within the abovementioned range [107]. As for the case of perovskite $RMnO_3$ (R = Dy, Ho, La, Pr, Nd, Tb and Bi), a common feature of the mild hydrothermal synthesis is the high alkalinity of the solutions. Such high alkalinity provides a critical condition, which considerably influences the crystallization and composition of the $RMnO_3$ product in the hydrothermal synthesis [108–109]. The high alkalinity of the reaction system also constitutes an optimal condition that considerably influences the crystallization of perovskite manganites. To maintain the suitable alkalinity required for the hydrothermal reaction, it is necessary to use a strong solvent such as KOH [110].

2.4.5. Synthesis of miscellaneous type perovskites and their solid solutions ($ANbO_3$, $ATaO_3$)

The solvent concentration also has an effect on the nucleation and crystal growth of other perovskite compounds, namely NN and KN ($NaNbO_3$, $KNbO_3$). The formation of this particular group of perovskites has been tailored in a media composed of a mixture of KOH

and NaOH solutions. The solvent has a composition assigned by the K^+:Na^+ molar ratio of 1:1, while the alkaline solvent solutions concentrations (NaOH or KOH) were 0.6, 0.8, 1.0 and 1.6 M. In the hydrothermal environment, OH^- ions exhibit a catalytic behaviour assisting the mass transport of the ionic solute species during the crystallization process. Also, these ions contribute to the particle nucleation and acceleration of the reaction [111]. However, when only NaOH was used as mineralizer, it was found that the reaction took place by an in situ transformation mechanism. The reaction speed was increased at low concentration of [OH^-] with increasing temperature. A high [OH^-] is not favourable to prepare perovskite NN, and there is an optimum [OH^-]. The concentration of [OH^-] and the reaction speed were correlated, which indicated that a high alkalinity is not useful for the synthesis of niobate [112]. In contrast, when a particular polymorph of Nb_2O_5 was selected as a precursor, the stability of the hexaniobate ion in solution was greater for lower KOH concentration and low temperature. In other words, the induction period related to the conversion of the hexaniobate ion to perovskite powder varied changing the concentration of KOH for a given temperature. Hence, it is possible to produce orthorhombic NN powders at 200°C using solutions of 8.4 M NaOH, 0.25 M Nb_2O_5 and KN powders; the reaction between solutions of different Nb_2O_5 concentrations (0.0015–0.38 M) and KOH (6.7–15 M) was only investigated at 200°C [113]. The reaction mechanism associated with the synthesis of AN is markedly different from that of NN reported in the literature. The heterogeneous chemical reaction between NH_4HF_2, Ag_2O, and Nb_2O_5 gives perovskite AN at pH = 3, adjusting the reaction media adding either an acidic solution (HF) or mild basic solution (NH_4OH). In the hydrothermal processing, water is not only used as the solvent for the crystallization of inorganic substances from solution, but other chemical processes also participate in the energy transfer, catalysis, dissolution and hydrolysis. The experimental results indicate that water solvent, as a solvent, provides a more powerful environment for the hydrothermal reactions for the crystallization of AN perovskites [114].

Cubic perovskite NT ($NaTaO_3$) powders were hydrothermally produced at 200°C for 24 h, employing a reaction medium with a concentration of 7 M and using KOH as mineralizer [115]. Due to the higher OH^- concentration contained in the hydrothermal system, a reaction by-product (pyrochlore) was obtained after the treatment. The pyrochlore crystalline phase subsequently reacted with the solvent media (KOH) to form a perovskite non-stoichiometric phase. In contrast, it was found that the reaction between Ta_2O_5 and NaOH for the synthesis of perovskite NT ($NaTaO_3$) powders follows the dissolution–recrystallization mechanism under microwave-assisted hydrothermal conditions. This reaction occurred without the addition of organic templates compounds and catalysts to the reaction medium. The thermodynamic energy barrier associated with the phase conversions, in this case, was estimated to be in the following order: $Ta_2O_5/Na_2Ta_2O_6$ < $NaTaO_3/Na_2Ta_2O_6$ < $Ta_2O_5/NaTaO_3$. A pretreatment of the Ta_2O_5 raw material by ball milling is a crucial step to obtain pure perovskite NT phase [116].

2.4.6. Synthesis of B site perovskite ($MeBO_3$)

At present, there are a few studies focused on the synthesis of ordered perovskites partially substituted at the B site. The synthesis of a few perovskite $MeBO_3$ group solid solutions have

http://dx.doi.org/10.5772/61568

been carried out under mild hydrothermal conditions, where the elements chosen were Me = Pb or Ba; B = Ti, Zr, Zn, or Ta, among others (hereafter these solid solutions are denominated as PZT, BTZ, BZT, respectively). These studies have been oriented to analyze the consolidation and functional properties of the synthesized materials, but any details were considered to clarify the chemical reaction pathways associated synthesis reaction that promotes the crystallization of these perovskite compounds. The present section of the review describes the conditions at which the synthesis of the perovskite solid solutions is possible to progress in a hydrothermal environment.

The hydrothermal processing procedure established for the synthesis of PZT perovskites involves the preparation of a hydrated mixed gel containing the main elements that constitute this compound. In this study, the factor exhaustively investigated was the molar Zr/Ti ratio. The effect of this parameter was considered to determine the optimum molar Zr/Ti ratio that chemically stabilizes the perovskite crystalline structure in different hydrothermal environments. As a consequence, the PZT single phase must belong to one of the three different crystalline structures, namely tetragonal, rhombohedral or pseudo-tetragonal [117]. The synthesis of PZT might occur in the sequence depicted by the chemical reactions that occur during the hydrothermal crystallization of PZT, represented by reactions 32 to 34:

$$PbO + 0.1\ TiO_2 \rightarrow \left(PbO : 0.1\ TiO_2\right)_{(s)} \tag{32}$$

$$2\left(PbO : 0.1\ TiO_2\right)_{ss} + 0.8\ TiO_{2(gel)} + ZrO_{2(gel)} \rightarrow 2Pb\left(Zr_{0.5}Ti_{0.5}\right)O_{3(amorphous)} \tag{33}$$

$$2Pb\left(Zr_{0.5}Ti_{0.5}\right)O_{3(amorphous)} \rightarrow 2Pb\left(Zr_{0.5}Ti_{0.5}\right)O_{3(s)} \tag{34}$$

The presence of H_2O under pressure (40–50 MPa) enhanced the solubility of TiO_2 in PbO, due to rapid transport of the ionic species in the supercritical fluid. In the KOH mild alkaline fluid between 160 and 350°C, PbO partially substituted with Ti rapidly reacts with the homogeneously dispersed precursor gel. The reaction accompanied by a progressive splitting off even large PbO particles (6 μm) occurred nearly the supercritical state of the hydrothermal media at 350°C by adjusting the solvent pH between 12 and 14. At this condition, the crystallization of the PZT tetragonal perovskite preferentially proceeded according to the chemical equilibrium that is given by Eq. (33). Therefore, the successful reactant mixing ratio Pb:Zr:Ti was 1:0.5:0.5, at which thermodynamically the hydrothermal media reach the equilibrium to achieve the crystallization of the tetragonal unit cell. The increase of the reaction time during the hydrothermal treatment provokes an increase in the crystallinity of the PZT product. It is well known that under hydrothermal treatment in an aqueous medium with basic pH (13.5), the hydroxide cation complexes of Pb, Zr and Ti undergoes a transition into PZT [118]. The crystallization of a nanocrystalline perovskite precursor phase was promoted using colloidal wet chemical processing and low-temperature crystallization stages. The common chemistry preparative procedure involves the co-precipitation of the precursor perovskite constituents

from a saturated solution. The co-precipitated colloid gel is obtained using an alkaline KOH solution with a concentration of 4 M producing a colloid suspension. The suspension containing the co-precipitated colloid (Pb-Zr-Ti-hydroxide) hydrothermally treated in an autoclave at 250°C for 5 h leads to prepare the tetragonal structured PZT particles exhibiting a cubic morphology and particle size of 600 nm [119]. On the other hand, the production of single crystal tetragonal perovskite PZT ($PbZr_{0.52}Ti_{0.48}O_3$) has been conducted adding a polymer compound. The process denominated as polymer-assisted hydrothermal synthesis was carried out at 200°C for 12 h. Among the polymer additives selected to control the micelles creation were PVA and PAA. The polymer plays an important role in the growth of PZT single crystals with tetragonal structure. The micelles tend to cover the faceted surfaces of the PZT particles, and this event produces a reduction in the superficial energy of the growing particles. Consequently, the PZT particles exhibit a preferential growth along the c axis of the tetragonal structure [120]. Besides the employment of water-soluble organic compounds aiming to control the particle crystal growth. A variety of organic bases provided another advantage for synthesizing PZT perovskites. The possibility to apply the organic bases as potential solid solvents in hydrothermal media was recently investigated in the preparation of PZT perovskite powders. The experiments were carried out in an alkali-free reaction media at 160°C for 72 h. The organic alkaline media selected to conduct the hydrothermal treatments was the tetramethylammonium hydroxide (TMAOH), this also operated as a pH-adjusting agent [121].

Other solid solutions of interest are the BTZ ($BaTi_{0.8}Zr_{0.2}O_3$) and the BZT ($BaZr_{1-x}Ti_xO_3$). The synthesis of these compounds at mild conditions has not been studied in detail yet. In one study conducted to prepare BTZ perovskite, a stoichiometric powdered mixture of Ti and Zr hydroxides, which was added to a 6 M $Ba(OH)_2$ solution. The barium saturated alkaline $Ba(OH)_2$ solution was selected as a solvent for the hydrothermal treatments to adjust the slurry before the hydrothermal synthesis. In this reaction media it was possible to carry out the crystallization of BZT particles with cubic structure, spherical morphology and molecular level homogeneous composition [122]. Likewise, BZT hollow nanospheres with cubic structure were synthesized at 200°C for 24 h using a KOH solution with a concentration of 16 M. The formation of the particles occurred due to Ostwald ripening mechanism, and the excess of Ti in the fluid may change the reaction mechanism that favours the hollowing process [123]. Finally, the synthesis reaction for the formation of BZnT ($BaZn_{1/3}Ta_{1/3}O_3$) was conducted in a reaction medium with a strong organic base (TMAOH), and the raw materials used were barium and zinc acetate, and tantalum oxalate solution. The reactions involved in the hydrothermal synthesis of the BZnT perovskite particles are reactions 35 to 37. Initially, in the first stage of the reaction occurred the decomposition of the organic alkaline produces a reduction in the total concentration of OH^- species at temperatures up to 150°C, simultaneously the nucleation of BZnT embryos occurred in the solution according to the chemical reaction Eq. (35). The decomposition of the TMAH to trimethylamine and methanol (Eq. 36) takes place at temperatures above 220°C in the hydrothermal vessel. The product trimethylamine is a weak alkali, and it has the same chemical reactivity such as that of the ammonia in an aqueous solution (Eq. 37), [124]. Hence, the low chemical stability of the organic alkaline might hinder the crystallization of the desired BZnT perovskite phase because the supersaturation state is difficult to reach in the reaction system.

http://dx.doi.org/10.5772/61568

$$3Ba\left(MeCO_2\right)_{2(aq)} + Zn\left(MeCO_2\right)_{2(aq)} + Ta_2O_5.xH_2O + 8NMe_4^+OH^-_{(aq)} \rightarrow 3BaZn_{1/3}Ta_{2/3}O_{3(s)} + 8\left(MeCO_2\right)^- NMe_4^+{}_{(aq)} + \left(4+x\right)H_2O_{(l)} \quad (35)$$

$$NMe_4^+OH^-_{(aq)} \rightarrow NMe_{3(aq)} + MeOH_{(aq)} \quad (36)$$

$$NMe_{3(aq)} + H_2O_{(l)} \Leftrightarrow NHMe_3^+{}_{(aq)} + OH^-_{(aq)} \quad (37)$$

2.4.7. Hydrothermal synthesis of AB site perovskites

The study of the synthesis of solid solutions with simultaneous substitutions in both locations (A and B sites) has been conducted under combined hydrothermal conditions. In a preliminary study, the synthesis of complex perovskite compounds (PBSZ and PBZT) was investigated using a KOH solution with concentrations varying in the range of 1.0–3.0 M. The elements that were partially incorporated into the ABX_3 structure were Pb, Ba and Sr added as A ions and Zr as B ion [125]. In the reaction media of KOH with concentrations of 2.0 and 3.0 M, most of the mixtures containing different contents of Ba and Sr were successfully crystallized and correspond to the tetragonal perovskite pure phase. However, the single perovskite phase was difficult to conduct in the alkaline solution with a concentration below 1 M. In conclusion, a hydrothermal media saturated with OH^- ions is usually required to prepare perovskite ternary compounds under hydrothermal conditions. On the other hand, the synthesis of modified lead titanate powder such as $(Pb_{0.88}Sm0._{08})(Ti_{0.99}Mn0_{.01})O_3$ has been conducted at pH between 8 and 12 using NaOH as mineralizer and metal nitrates precursor solutions. The conditions that favour the crystallization of the perovskite structure are 290°C for 10 h at a pH = 10 [126]. In general, the vast number of studies discussed in the preliminary sections, regarding the synthesis of several groups of perovskite compounds, indicate that the processing parameters (precursor metal salts reagents, solvent media, pH of the precursor solution, reaction time, and temperature) must be carefully selected to carry on the processing perovskite compounds either by hydrothermal microwave-assisted synthesis, hydrothermal surfactant-assisted synthesis or supercritical water conditions.

2.5. Summary

This review describes in detail the state-of-the-art regarding the theoretical and practical aspects associated with the synthesis of a wide number of perovskite-structured compounds. The use of the thermodynamic and kinetic modelling has proved to be a powerful tool to optimize the conditions for perovskite compounds under hydrothermal conditions. These tools allow in a rational way to engineer the processing of smart perovskite compounds, in the most cost-effective approach and an environmental friendly way as well. One of the particular advantages of hydrothermal processing is associated with the preparation of monodispersed nanometer-sized particles exhibiting a control over their shape and size in addition to their chemical homogeneity. However, the models discussed in the present review are only

applicable to a very narrow boundary of experimental conditions in which the heterogeneous hydrothermal reaction equilibriums are achieved, namely in the pH range from 0 to 14. The vast practical expertise gained from the past three decades in the synthesis of a wide number of perovskite-structured compounds using the hydrothermal technique indicates that some caution must be executed, when applying the proposed models to diverse perovskite systems. The results derived from the kinetics and thermodynamical models might vary depending on the reaction temperature, concentration of precursors and the alkalinity of the hydrothermal media. Therefore, more conscious analyses based on inorganic chemistry fundamentals coupled with chemical engineering and kinetic modelling might help to derive the adequate conditions to achieve controlled crystallization of particles with specific particle size and morphology. Although the present information regarding the hydrothermal synthesis of perovskite compounds, in terms of the theoretical and practical approaches, has been evaluated with a high statistical reproducibility in small-scale laboratory reactors, there is a potential field to explore when scaling up the process to larger industrial reactors, where mixing problems might frequently raise due to slow and less-efficient agitation systems. Mixing-limited precipitation rate is one of the problems commonly encountered in the scale-up of precipitation processes.

Author details

Juan Carlos Rendón-Angeles[1*], Zully Matamoros-Veloza[2], Karla Lorena Montoya-Cisneros[1], Jorge López Cuevas[1] and Kazumichi Yanagisawa[3]

*Address all correspondence to: jcarlos.rendon@cinvestav.edu.mx

1 Research Institute for Advanced Studies of the NPI, Ceramic Department, Ramos Arizpe, Coahuila, México

2 Technological Institute of Saltillo, Metal-Mechanics Department, Saltillo, Coahuila, México

3 Research Laboratory of Hydrothermal Chemistry, Kochi University, Kochi, Japan

References

[1] Mohammad HH. Characterisation of Mixed-Metal Oxides Prepared by Hydrothermal Synthesis. [thesis]. Coventry CV4 7AL, United Kingdom: The University of Warwick; 2013.

[2] Mats J, Peter L. Crystallography and Chemistry of Perovskites. Handbook of Magnetism and Advanced Magnetic Materials. p. 2007. DOI: 10.1002/9780470022184.hmm411

[3] Kay HF, Bailey PC. Structure and properties of $CaTiO_3$. Acta Crystallogr 1957;10:219–26. DOI:10.1107/S0365110X57000675

[4] Sasaki S, Prewitt CT, Bass JD, Schulze WA. Orthorhombic perovskite $CaTiO_3$ and $CdTiO_3$: structure and space group. Acta Crystallogr 1987;C43:1668–74. DOI:10.1107/S0108270187090620

[5] Verma AS, Jindal VK. ABX_3 type oxides and halides: their structure and physical properties. In: Perovskites: Structure, Properties and Uses. Editors: Maxim Borowski, Editorial: 2010, Chapter: 11. pp. 463–479. DOI: 10.1002/chin.201121201

[6] John BG, Zhou JS. Orbital ordering in orthorhombic perovskites. J Mater Chem 2007;17:2394–405. DOI: 10.1039/b701805c

[7] Nicole AB, Craig JF. Why are there so few perovskite ferroelectrics? J Phys Chem 2013;117:13339−49. DOI.org/10.1021/jp402046t

[8] Ivan AS, Cengiz S, Elbio D. Ferroelectricity in the magnetic *E*-phase of orthorhombic perovskites. Phys Rev Lett 2006;97:227204-1–227204-4. DOI:10.1103/PhysRevLett.97.227204

[9] Goodenough JB, Longo JM. In: Landolt-Cornstein. Numerical data and functional relationships in science and technology, new series, group III: crystal and solid state physics. Magnetic and other properties of oxides and related compounds, part A, vol. 4. Berlin: Springer; 1970. p. 126.

[10] Warren EP, David JS. Electronic structure and half-metallic transport in the $La_{1-x}Ca_xMnO_3$ system. PRB 1996;53,3:1146–60. DOI: 10.1103/PhysRevB.53.1146

[11] Goodenough JB, Longo JM. Crystallographic and magnetic properties of perovskite and perovskite – related compounds. In: LANDOLT-BÖRNSTEIN Zahlenwerte und Funktionen aus Naturwissenschaften und Technik. Neue Serie. Gesamtherausgabe: K.-H. Hellwege. Band 4 Magnetische und andere Eigennschaften von Oxiden und werwandten Verbindungen. Spring-Verla; 1970. pp. 126–129.

[12] Wiebe CR, Greedan JE, Kyriakou PP, Luke GM, Gardner JS, Fukaya A, Gat-Malureanu IM, Russo PL, Savici AT, Uemura YJ. Frustration-driven spin freezing in the S= ½ fcc perovskite Sr_2MgReO_6. PRB 2003;68:134410-1–134410-10. DOI: 10.1103/PhysRevB.68.134410

[13] Cava RJ, Batlogg B, Krajewski JJ, Farrow R, Rupp Jr LW, White AE, Short K, Peck WF, Kometani T. Superconductivity near 30 K without copper: the $Ba_{0.6}K_{0.4}BiO_3$ perovskite. 1988;332:814:814–816. DOI:10.1038/332814a0

[14] Sami V, Maarit K. $A_2B'B''O_6$ perovskites: a review Prog Solid State Chem 2015;43:1–36. http://dx.doi.org/10.1016/j.progsolidstchem.2014.08.001

[15] Eduardo CCdeS, Reginaldo M. Properties and applications of perovskite proton conductors. Mater Res 2010;13(3):385–94. http://dx.doi.org/10.1590/S1516-14392010000300018

[16] Peña MA, Fierro JLG. Chemical structures and performance of perovskite oxides. Chem Rev 2001;101:1981–2017. DOI: 10.1021/cr980129f

[17] Bonanos N, Knight KS, Ellis B. Perovskite solid electrolytes: structure, transport properties and fuel cell applications. Solid State Ionics 1995;79:161–70. DOI 10.1016/0167-2738(95)00056-C

[18] Stephen JS. Recent advances in perovskite-type materials for SOFC cathodes. Fuel Cells Bull 2001;4(33):6–12. DOI: 10.1016/S1464-2859(01)80254-6

[19] Stephen JS. Recent advances in Perovskite-type materials for solid oxide fuel cell cathodes. Int J Inorg Mater 2001;3:113–21. DOI:10.1016/S1466-6049(01)00004-6

[20] Harlan UA. Review of p-type doped perovskite materials for SOFC and other applications. Solid State Ionics 1992;52(1–3):33–41. DOI: 10.1016/0167-2738(92)90089-8

[21] Bangerta U, Falke U, Weidenkaff A. Ultra-high resolution EEL studies of domains in Perovskite. J Phys Conf Ser 2006;26:17–20. DOI:10.1088/1742-6596/26/1/004.

[22] Tapas KM, Gopalakrishnan J. From rocksalt to perovskite: a metathesis route for the synthesis of perovskite oxides of current interest. J Mater Chem 2004;14:1273–80. DOI: 10.1039/b315263d

[23] Hans-Conrad zL, Qingbiao Z, Daniel EB, Michael WC. 2H-perovskite related oxides: Synthesis, structures, and predictions. Cryst Eng Comm 2012;14:23–39. DOI: 10.1039/c1ce05788j

[24] Jesús P-G, Rainer S, Emilio M. Microwave-assisted synthesis and characterization of perovskite oxides. In: Jinghua Z, Huan L, eds. Perovskite: Crystallography, Chemistry and Catalytic Performance. Novascience Publishers, Hauppauge (USA) 2013. pp. 117–140. DOI: 10.1002/chin.201424225

[25] Parkin IP, Solid state metathesis reaction for metal borides, silicides, pnictides and chalcogenides: ionic or elemental pathways. Chem Soc Rev 1996;25:199–207, DOI: 10.1039/CS9962500199

[26] Stanley MW. Hydrothermal synthesis of transition metal oxides under mild conditions. Solid State Mater Sci 1996;1[2]:227–32. DOI: 10.1016/S1359-0286(96)80089-1

[27] Thierry D, Ali A-Z, Berger M-H, Xavier B, Hochepied J-E. Hydrothermal synthesis of ferroelectric mixed potassium niobate–lead titanate nanoparticles. J Am Ceram Soc 2014;97[5]:1456–64. DOI: 10.1111/jace.12778

[28] Stefan GE, Abicht H-P, Dronskowski R, Müller T, Reller A, Weidenkaff A. Perovskite-related oxynitrides – recent developments in synthesis, characterisation and in-

vestigations of physical properties. Prog Solid State Chem 2009;37:173–205. DOI: 10.1016/j.progsolidstchem.2009.11.003

[29] David S. Related chemical themes in the synthesis of advanced ceramic materials. Mater Sci Eng 1989;A109:261–4. ISBN: 9780521424189

[30] Muthurajan H, Kumar HH, Samuel V, Gupta UN, Ravi V. Novel hydroxide precursors to prepare $NaNbO_3$ and $KNbO_3$. Ceram Int 2008;34:671–3. DOI:10.1016/j.ceramint.2006.12.014

[31] Irena P, Darko M, Miha D. Chemical synthesis of $KNbO_3$ and $KNbO_3$–$BaTiO_3$ ceramics. J Eur Ceram Soc 2005;25:2713–7. DOI:10.1016/j.jeurceramsoc.2005.03.128

[32] Bhattacharyya K, Tyagi AK. A novel soft-chemical method for the synthesis of nanocrystalline $MNbO_3$ (M=Na, K). J Alloys Compd 2009;470:580–3. DOI:10.1016/j.jallcom.2008.03.024

[33] Meinan L, Dongfeng X, Shouchen Z, Haiyang Z, Jiyang W, Kenji K. Chemical synthesis of stoichiometric lithium niobate powders. Mater Lett 2005;59:1095–7.

[34] Lu C-H, Lo S-Y, Wang Y-L. Glycothermal preparation of potassium niobate ceramic particles under supercritical conditions. Mater Lett 2002;55:121–5. DOI:10.1016/S0167-577X(01)00633-4

[35] Byrappa K. Hydrothermal Processing. Kirk-Othmer Encyclopedia of Chemical Technology. Wiley; 2005. pp. 1–43. DOI: 10.1002/0471238961.0825041804012319.a01.pub2. ISBN 9780471238966

[36] Byrappa K, Masahiro Y. Hydrothermal technology—principles and applications. In: Gary EM, Stephen MR, Roitan FB, eds. Handbook of Hydrothermal Technology. Technology for Crystal Growth and Materials Processing. William Andrew Publishing/ Noyes Publications. 2001. 11 p. ISBN 0-8155-1445-X

[37] Suchanek WL, Lencka MM, Riman RE. Hydrothermal Synthesis of ceramic materials. In: Donald AP, Roberto F-P, Allan HH, eds. Aqueous System at Elevated Temperature and Pressures: Physical Chemistry in Water, Steam and Hydrothermal Solutions. Elsevier; 2004. pp. 717–744. ISBN: 978-0-12-544461-3

[38] Malgorzata ML, Richard ER. Intelligent synthesis of smarteramic materials. In: Mel S, ed. Encyclopedia of Smart Materials. Volume 1. John Wiley. 2002. pp. 568–580. ISBN 0471177806, 9780471177807

[39] Byrappa K, Adschiri T. Hydrothermal technology for nanotechnology. Prog Crystal Growth Character Mater 2007;53:117–66. DOI:10.1016/j.pcrysgrow.2007.04.001

[40] Malgorzata ML, Richard ER. Thermodynamic modeling of hydrothermal synthesis of ceramic powders. Chem Mater 1993;5(1):61–70. DOI: 10.1021/cm00025a014

[41] Malgorzata ML, Richard ER. Thermodynamics of the hydrothermal synthesis of calcium titanate with reference to other alkaline-earth titanates. Chem Mater 1995;7[1]: 18–25. DOI: 10.1021/cm00049a006

[42] Malgorzata ML, Richard ER. Hydrothermal synthesis of Perovskite materials: Thermodynamic modeling and experimental verification. Ferroelectrics 1994;151:159–64. DOI: 10.1080/00150199408244737

[43] Malgorzata ML, Erik N, Andrzej A, Richard ER. Hydrothermal synthesis of carbonate-free strontium zirconate: thermodynamic modeling and experimental verification. Chem Mater 1997;9[5]:1116–25 DOI: 10.1021/cm960444n

[44] Malgorzata ML, Richard ER. Synthesis of lead titanate: thermodynamic modeling and experimental verification. J Am Ceram Soc 1993;76[10]:2649–59. DOI: 10.1111/j.1151-2916.1993.tb03994.x

[45] Cho S-B, Noh J-S, Malgorzata ML, Richard ER. Low temperature hydrothermal synthesis and formation mechanisms of lead titanate ($PbTiO_3$) particles using tetramethylammonium hydroxide: thermodynamic modelling and experimental verification. J Eur Ceram Soc 2003;23:2323–35. DOI:10.1016/S0955-2219(03)00085-2

[46] Gelabert MC, Laudise RA, Riman RE. Phase stability, solubility and hydrothermal crystal growth of $PbTiO_3$. J Cryst Growth 1999;197[1–2]:195–203. DOI: 10.1016/S0022-0248(98)00914-2

[47] James OE, Jr, Catherine CH-H, Bonnie LG, Malgorzata ML, Richard R. Kinectics and mechanism of hydrothermal synthesis of barium titanate. J Am Ceram Soc 1996;79[11]:2929–39. DOI: 10.1111/j.1151-2916.1996.tb08728.x

[48] Bonnie LG, Malgorzata ML, Richard ER. Low-temperature hydrothermal synthesis of phase-pure (Ba,Sr)TiO_3 perovskite using EDTA. J Am Ceram Soc 2004;87[11]:2025–32. DOI: 10.1111/j.1151-2916.2004.tb06355.x

[49] Malgorzata ML, Andrzej A, Richard ER. Hydrothermal precipitation of lead zirconate titanate solid solutions: thermodynamic modeling and experimental synthesis. J Am Ceram Soc 1995;78[10]:2609–18. DOI: 10.1111/j.1151-2916.1995.tb08030.x

[50] Andrea T, Vincenzo B, Maria TB, Massimo V, Paolo N. Kinetic modeling of aqueous and hydrothermal synthesis of barium titanate ($BaTiO_3$). Chem Mater 2005;17[21]: 5346–56. DOI: 10.1021/cm051119f

[51] Andrea T, Maria TB, Vincenzo B, Massimo V, Carlo B, Paolo N. Kinetics and mechanism of aqueous chemical synthesis of $BaTiO_3$ particles. Chem Mater 2004;16[8]:1536–43. DOI: 10.1021/cm031130k

[52] Daniele LM. On the use of bi-variate population balance equations for modelling barium titanate nanoparticle precipitation. Chem Eng Sci 2009;64:697–708. DOI:10.1016/j.ces.2008.04.052

[53] Ouchiyama N, Rough SL, Bridgwater J. Apopulation balance approach to describing bulk attrition. Chem Eng Sci 2005;60:1429–40. DOI:10.1016/j.ces.2004.08.037

[54] Doraiswami R, Alan WM. Population balance modeling. Promise for the future. Chem Eng Sci 2002;57[4]:595–606. DOI: 10.1016/S0009-2509(01)00386-4.

[55] Lee W, Kim HK, Cho SB. Hydrothermal preparation of $BaTiO_3$ powders from modified hydroxide precursors. Ferroelectrics 2006;333:233–41. DOI: 10.1080/00150190600701319

[56] Changlong C, Yuling W, Xiuling J, Dairong C. Hydrothermal synthesis of $BaTiO_3$: Crystal phase and the Ba^{2+} ions leaching behavior in aqueous médium. Mater Chem Phys 2008;110:186–91. DOI:10.1016/j.matchemphys.2008.01.031

[57] Durrani SK, Naz S, Hayat K. Thermal analysis and phase evolution of nanocrystalline perovskite oxide materials synthesized via hydrothermal and self-combustion methods. J Therm Anal Calorim 2014;115:1371–80. DOI 10.1007/s10973-013-3452-1

[58] Wen C, Tingke R, Aiwu W, Jie H, Junqing W, Jiasong Z, Weidong X. A simple and controllable hydrothermal route for the synthesis of monodispersed cube-like barium titanate nanocrystals. Ceram Int 2015;41:4514–22. http://dx.doi.org/10.1016/j.ceramint.2014.11.146

[59] Jooho M, Jeffrey AK, Henrik K, James HA. Hydrothermal synthesis of ferroelectric perovskites from chemically modified titanium isopropoxide and acetate salts. J Mater Res 1999;14[2]:425–35. DOI: 10.1557/JMR.1999.0061

[60] Lee S-K, Choi G-J, Hwang U-Y, Koo K-K, Park T-J. Effect of molar ratio of KOH to Ti-isopropoxide on the formation of $BaTiO_3$ powders by hydrothermal method. Mater Lett 2003;57:2201–7. DOI:10.1016/S0167-577X(02)01174-6

[61] Xiao W, Gang X, Zhaohui R, Yonggang W, Ge S, Gaorong H. Size-controlled synthesis of $BaTiO_3$ nanocrystals via a hydrothermal route. Mater Lett 2008;62:3666–9. DOI: 10.1016/j.matlet.2008.04.022

[62] Yonggang W, Gang X, Linlin Y, Zhaohui R, Xiao W, Wenjian W, Piyi D, Ge S, Gaorong H. Hydrothermal synthesis of single-crystal $BaTiO_3$ dendrites. Mater Lett 2009;63:239–41. DOI:10.1016/j.matlet.2008.09.050

[63] Xinhua Z, Junyi W, Zhenghai Z, Jianmin Z, Shunhua Z, Zhiguo L, Naiben M. Perovskite nanoparticles and nanowires: microwave–hydrothermal synthesis and structural characterization by high-resolution transmission electron microscopy. J Am Ceram Soc 2008;91:2683–9. DOI: 10.1111/j.1551-2916.2008.02494.x

[64] Lan X, Kongjun Z, Jing W, Qilin G, Yang C, Hongjuan Z, Jinsong L, Jinhao Q. Microwave-assisted sol–hydrothermal synthesis of tetragonal barium titanate nanoparticles with hollow morphologies. J Mater Sci Mater Electron 2015;26:1597–601. DOI: 10.1007/s10854-014-2581-z

[65] Ohara Y, Koumoto K, Shimizu T, Yanagida H. Hydrotherrnal synthesis of fibrous lead titanate Powders. J Mater Sci 1995;30:263–6. DOI 10.1007/BF00352160

[66] Gang X, Xiaoqiang H, Vladimir K, Shuquan C, Xin Y, Chunying C, Ge S, Gaorong H. Hydrothermal synthesis of single-crystalline tetragonal perovskite $PbTiO_3$ nanosheets with dominant (001) or (111) facets. Cryst Eng Comm 2014;16:4373–6. DOI: 10.1039/c4ce00234b

[67] Mario LM, Elaine CP, Gabriela SdN, Valeria ML, Julio RS, Valmor RM, Maria IBB, Juan A, José AV, Elson L. Structural and optical properties of $CaTiO_3$ perovskite-based materials obtained by microwave-assisted hydrothermal synthesis: an experimental and theoretical insight. Acta Mater 2009;57:5174–85. DOI:10.1016/j.actamat.2009.07.019

[68] Tatiana MM, Mario LM, Ivo MP, Francini CP, Edson RL, Ieda LVR, José AV, Leinig AP, Elson L. $CaTiO_3:Eu^{3+}$ obtained by microwave assisted hydrothermal method: A photoluminescent approach. Opt Mater 2010;32:990–7. DOI:10.1016/j.optmat.2010.01.039

[69] Yonggang W, Gang X, Linlin Y, Zhaohui R, Xiao W, Wenjian W, Piyi D, Ge S, Gaorong H. Formation of single-crystal $SrTiO_3$ dendritic nanostructures via a simple hydrothermal method. J Cryst Growth 2009;311:2519–23. DOI:10.1016/j.jcrysgro.2009.01.103

[70] Rangel-Hernandez YM, Rendón-Angeles JC, Matamoros-Veloza Z, Pech-Canul MI, Diaz-de la ST, Yanagisawa K. One-step synthesis of fine $SrTiO_3$ particles using $SrSO_4$ ore under alkaline hydrothermal conditions. Chem Eng 2009;155:483–92. DOI: 10.1016/j.cej.2009.07.024

[71] Xiao W, Gang X, Zhaohui R, Ge S, Gaorong H. Effect of KOH concentration on the phase and morphology of hydrothermally synthesized $Pb_{0.70}La_{0.30}TiO_3$ fine powders. Mater Lett 2008;62:3719–21. DOI:10.1016/j.matlet.2008.04.039

[72] Jean-François T, Sophie d'A, Christian C, Philippe C, Mohamed R, Anne L. Influence of hydrothermal synthesis conditions on BNT-based piezoceramics. J Eur Ceram Soc 2011;31:1997–2004. DOI:10.1016/j.jeurceramsoc.2011.04.025

[73] Jianhong P, Mirabbos H, Baowei C, Juan W, Yunhua X. Surfactant-free hydrothermal synthesis of submicron $BiFeO_3$ powders. Appl Phys A 2011;103:511–6. DOI 10.1007/s00339-010-6024-2

[74] Xin Y, Gang X, Zhaohui R, Xiao W, Chunying C, Siyu G, Ge S, Gaorong H. The hydrothermal synthesis and formation mechanism of single-crystalline perovskite $BiFeO_3$ microplates with dominant (012) facets. Cryst Eng Comm 2014;16:4176–82. DOI: 10.1039/c3ce42488j

[75] Xian-Zhi C, Zhong-Cheng Q, Jian-Ping Z, Gangqiang Z, Xiao-Bing B, Peng L. Large-scale growth and shape evolution of bismuth ferrite particles with a hydrothermal method. Mater Chem Phys 2011;126:560–7. DOI:10.1016/j.matchemphys.2011.01.027

[76] Chao C, Jinrong C, Shengwen Y, Lingjuan C, Zhongyan M. Hydrothermal synthesis of perovskite bismuth ferrite crystallites. J Cryst Growth 2006;291:135–9. DOI: 10.1016/j.jcrysgro.2006.02.048

[77] Hong J, Yasutaka M, Nobuhiro K, Yoshinnori Y, Takahiro T, Nobukazu K. Hydrothermal synthesis of perovskite-type $BiFeO_3$. J Ceram Soc Jpn 2008;116[7]:837–9.

[78] Yonggang W, Gang X, Zhaohui R, Xiao W, Wenjian W, Piyi D, Ge S, Gaorong H. Low temperature polymer assisted hydrothermal synthesis of bismuth ferrite nanoparticles. Ceram Int 2008;34:1569–71. DOI:10.1016/j.ceramint.2007.04.013

[79] Chun YS, Jinbao X, Aerpati Y, Lei W. Hydrothermal synthesis of perovskite bismuth ferrite micro/nano powders. Integr Ferroelect 2014;153:33–41. DOI: 10.1080/10584587.2014.902668

[80] Zhiwu C, Yongpeng W, Jianqiang H. Ethanol-assisted hydrothermal synthesis and characterization of $BiFeO_3$ nanopowders. J Am Ceram Soc 2013;96[5]:1345–8. DOI: 10.1111/jace.12296

[81] Zhiwu C, Wuliang J. Low-temperature acetone-assisted hydrothermal synthesis and characterization of $BiFeO_3$ powders. J Mater Sci: Mater Electron 2014;25:4039–45. DOI 10.1007/s10854-014-2126-5

[82] Hongbin Q, Hailong Z, Bo-Ping Z, Lihua X. Hydrothermal synthesis of perovskite $BiFeO_3$–$BaTiO_3$ crystallites. J Am Ceram Soc 2011;94[11]:3671–4. DOI: 10.1111/j.1551-2916.2011.04839.x

[83] Zhiqiang Z, Li G, Haixia Y, Qiang L, Feng Y. Hydrothermal synthesis and magnetic properties of multiferroic rare-earth orthoferrites. J Alloys Compd 2014;583:21–3. http://dx.doi.org/10.1016/j.jallcom.2013.08.129

[84] Youjin Z, Ao Z, Xiaozhi Y, Hongmei H, Yun F, Chengpeng Y. Cubic $GdFeO_3$ particle by a simple hydrothermal synthesis route and its photoluminescence and magnetic properties. Cryst Eng Comm 2012;14:8432–9. DOI: 10.1039/c2ce26233a

[85] Mingyu S, Chenyang Z, Tingsong Z, Lin Y, Lei G, Hongming Y, Shouhua F. The multiferroic perovskite $YFeO_3$. Appl Phys Lett 2013;102:062903-1–062903-4. http://dx.doi.org/10.1063/1.4791697

[86] Guo-Qiang T, Yu-Qin Z, Hong-Yan M, Ao X, Hui-Jun R. Controllable microwave hydrothermal synthesis of bismuth ferrites and photocatalytic characterization. J Am Ceram Soc 2012;95[1]:280–9. DOI: 10.1111/j.1551-2916.2011.04775.x

[87] Biasotto GB, Simoes AZ, Foschini CR, Zaghete MA, Varela JA, Longo E. Microwave-hydrothermal synthesis of perovskite bismuth ferrite nanoparticles. Mater Res Bull 2011;46:2543–7. DOI:10.1016/j.materresbull.2011.08.010

[88] Zhi W, Wenfei X, Hui P(a), Xiaodong T(b). Polyanion modulated evolution of perovskite $BiFeO_3$ microspheres to microcubes by a microwave assisted hydrothermal method. J Mater Res 2013;28[11]:1498–504. DOI: 10.1557/jmr.2013.130

[89] Millot N, Xin B, Pighini C, Aymes D. Hydrothermal synthesis of nanostructured inorganic powders by a continuous process under supercritical conditions. J Eur Ceram Soc 2005;25:2013–6. DOI: 10.1016/j.jeurceramsoc.2005.03.202

[90] Aimable A, Xin B, Millot N, Aymes D. Continuous hydrothermal synthesis of nanometric $BaZrO_3$ in supercritical water. J Solid State Chem 2008;181:183–9. DOI: 10.1016/j.jssc.2007.11.015

[91] Zhouguang L, Yougen T, Limiao C, Yadong L. Shape-controlled synthesis and characterization of $BaZrO_3$ microcrystals. J Cryst Growth 2004;266:539–44. DOI: 10.1016/j.jcrysgro.2004.02.107

[92] Jia G, Guo Z, Jianguo Y, Yongcun Z, Guodong L, Guangshan Z, Yongnan Z. Fabrication and luminescence properties of $Rb_xBa_{1-x}ZrO_3$ hollow nanospheres. Mater Lett 2014;116:164–6. http://dx.doi.org/10.1016/j.matlet.2013.11.002

[93] Wenjun Z, Wenqin P, Guangyao M, Dingkun P. Hydrothermal synthesis and characterization of $LaCrO_3$. J Mater Chem 1999;9:2833–6. DOI: 10.1039/A904399C

[94] Bo HC, Shin-Ae P, Bong KP, Ho HC, Yong-Tae K. Controlled synthesis of $La_{1-x}Sr_xCrO_3$ nanoparticles by hydrothermal method with nonionic surfactant and their ORR activity in alkaline médium. Mater Res Bull 2013;48:3651–6. http://dx.doi.org/10.1016/j.materresbull.2013.04.084

[95] Rendón-Angelesa JC, Yanagisawa K, Matamoros-Veloza Z, Pech-Canula MI, Mendez-Nonell J, Diaz-de la ST. Hydrothermal synthesis of perovskite strontium doped lanthanum chromite fine powders and its sintering. J Alloys Compd 2010;504:251–6. DOI: 10.1016/j.jallcom.2010.05.103

[96] Shan W, Keke H, Beining Z, Jiaqi Z, Shouhua F. Mild hydrothermal synthesis and physical property of perovskite Sr doped $LaCrO_3$. Mater Lett 2013;101:86–9. http://dx.doi.org/10.1016/j.matlet.2013.03.083

[97] Kripasindhu S, Martin RL, Reza JK, Jeremy S, Richard IW. Direct hydrothermal synthesis and physical properties of rare-earth and yttrium orthochromite perovskites. Chem Mater 2011;23:48–56. DOI: 10.1021/cm102925z

[98] Deliang Z, Hong Z, Yuheng Z. Hydrothermal synthesis of $La_{0.5}Ba_{0.5}MnO_3$ nanowires. Appl Phys Lett 2002;80[9]:1634–6. DOI: 10.1063/1.1455690#

[99] Zhang T, Jin CG, Qian T, Lu XL, Bai JM, Li XG. Hydrothermal synthesis of single-crystalline $La_{0.5}Ca_{0.5}MnO_3$ nanowires at low temperature. J Mater Chem 2004;14:2787–9. DOI: 10.1039/b405288a

[100] Bernard C, Dauzet G, Mathieu F, Durand B, Puech-Costes E. Optimization of the hydrothermal synthesis of $La_{0.7}Sr_{0.3}MnO_{3+\delta}$ using an original optimal experimental design. Mater Lett 2005;59:2615–20. DOI: 10.1016/j.matlet.2005.02.063

[101] Darko M, Tanja G, Klementina Z, Darja L. Hydrothermal synthesis of $La_{1-X}Sr_XMnO_3$ dendrites. J Cryst Growth 2013;375:78–83. http://dx.doi.org/10.1016/j.jcrysgro.2013.04.019

[102] Jeroen S, Richard IW, Franck M. A study of the manganites $La_{0.5}M_{0.5}MnO_3$ (M=Ca, Sr, Ba) prepared by hydrothermal synthesis. J Mater Chem 2005;15:1542–51. DOI: 10.1039/b417003b

[103] Sun WA, Li JQ, Ao WQ, Tang JN, Gong XZ. Hydrothermal synthesis and magnetocaloric effect of $La_{0.7}Ca_{0.2}Sr_{0.1}MnO_3$. Powder Technol 2006;166(2):77–80. DOI: 10.1016/j.powtec.2006.05.015

[104] Li JQ, Sun WA, Ao WQ, Tang JN. Hydrothermal synthesis and Magnetocaloric effect of $La_{0.5}Ca_{0.3}Sr_{0.2}MnO_3$. J Magnet Magnet Mater 2006;302:463–6. http://dx.doi.org/10.1016/j.jmmm.2005.10.007

[105] Simon I, Akim K, Patrick G, Didier L. Conventional hydrothermal process versus microwave-assisted hydrothermal synthesis of $La_{1-x}Ag_xMnO_{3+\delta}$ (x=0, 0.2) perovskites used in methane combustion C R Chim 10 2007;10:1216–26. http://dx.doi.org/10.1016/j.crci.2007.08.002

[106] Zhiqiang Z, Li G, Feng Y, Hydrothermal synthesis, magnetism and resistivity of orthorhombic perovskite manganates $Y_{1-x}Ca_xMnO_3$ (x=0, 0.007, 0.55, 0.65). J Alloys Compd 2013;571:123–31.http://dx.doi.org/10.1016/j.jallcom.2013.03.220

[107] Jeroen S, Richard IW. Hydrothermal synthesis of the perovskite manganites $Pr_{0.5}Sr_{0.5}MnO_3$ and $Nd_{0.5}Sr_{0.5}MnO_3$ and alkali-earth manganese oxides $CaMn_2O_4$, 4H-$SrMnO_3$, and 2H-$BaMnO_3$. J Solid State Chem 2005;178:1683–91. http://dx.doi.org/10.1016/j.jssc.2005.03.006

[108] Yongwei W, Xiaoying L, Yan C, Fangli C, Shouhua F, Xiaoyang L, Hydrothermal synthesis of two perovskite rare-earth manganites, $HoMnO_3$ and $DyMnO_3$. J Solid State Chem 2005;178:1317–20. http://dx.doi.org/10.1016/j.jssc.2004.12.039

[109] Yan C, Hongming Y, Ge T, Ganghua Z, Shouhua F. Hydrothermal synthesis and magnetic properties of RMn_2O_5 (R=La, Pr, Nd, Tb, Bi) and $LaMn_2O_{5+\delta}$. J Solid State Chem 2007;180[4]:1340–6. http://dx.doi.org/10.1016/j.jssc.2007.02.005

[110] Yan C, Hongming Y, Guanghua L, Ge T, Shouhua F. Crystal growth and magnetic property of orthorhombic $RMnO_3$ (R=Sm–Ho) perovskites by mild hydrothermal

synthesis. J Cryst Growth 2007;305[1]:242–8. http://dx.doi.org/10.1016/j.jcrysgro.2007.03.052

[111] Kongjun Z, Yang C, Xiaohui W, Lin B, Jinhao Q, Hongli J. Hydrothermal synthesis of sodium niobate with controllable shape and structure. Cryst Eng Comm 2012;14:411–6. DOI: 10.1039/C1CE06100C

[112] Wu SY, Zhang W, Chen XM. Formation mechanism of $NaNbO_3$ powders during hydrothermal synthesis. J Mater Sci Mater Electronics 2010;21[5]:450–5. DOI: 10.1007/s10854-009-9937-9

[113] Gregory KLG, Fred FL, Sossina MH, Carlos GL, Gregory KLG, Fred FL, Sossina MH, Carlos GL. Hydrothermal synthesis of $KNbO_3$ and $NaNbO_3$ powders. J Mater Res 2003;18[2]:338–45. DOI: 10.1557/JMR.2003.0044

[114] Haibo C, Mingyu S, Chenyang Z, Hongming Y, Shouhua F. Hydrothermal syntheses and structural phase transitions of $AgNbO_3$. J Am Ceram Soc 2012;95[11]:3673–77. DOI: 10.1111/j.1551-2916.2012.05392.x

[115] Gregory KLG, Sossina MH, Carlos GL, Fred FL. Hydrothermal synthesis of perovskite and pyrochlore powders of potassium tantalate. J Mater Res 2002;17:3168–76. DOI: 10.1557/JMR.2002.0458

[116] Jingying S, Guiji L, Nan W, Can L. Microwave-assisted hydrothermal synthesis of perovskite $NaTaO_3$ nanocrystals and their photocatalytic properties. J Mater Chem 2012;22:18808–13. DOI: 10.1039/c2jm33470d

[117] Kutty TRN, Balachandran R. Direct precipitation of lead zirconate titanate by the hydrothermal method. Mat Res Bull 1984;19:1479–88.

[118] Anjali AA, Malini SB. Synthesis of nanocrystalline PZT by hydrothermal method. Defence Sci J 2007;57[1]:35–9.

[119] Ralph N, Norbert BH. Hydrothermal synthesis of nanocrystalline perovskite powder systems. Mol Cyst Liq Cfysr 2000;353:329–40.

[120] Gang X, Zhaohui R, Piyi D, Wenjian WE, Ge S, Gaoirong H. Polymer-assisted hydrothermal synthesis of single-crystalline tetragonal perovskite $PbZr_{0.52}Ti_{0.48}O_3$ nanowires. Adv Mater 2005;17[7]:907–10. DOI: 10.1002/adma.200400998

[121] Ivan P, Malgorzata ML, Andrzej A, Richard ER. Hydrothermal synthesis of lead zirconate titanate ($PbZr_{0.52}Ti_{0.48}O_3$) using organic mineralizers. In: Applications of Ferroelectrics, 1996. ISAF '96, Proceedings of the Tenth IEEE International Symposium on (Volume:2); 18–21 Aug 1996; East Brunswick, NJ: ieee; DOI: 10.1109/ISAF.1996.598129

[122] Fukai K, Hidaka K, Aoki M, Abe K. Preparation and properties of uniform fine perovskite powders by hydrothermal synthesis. Ceram Int 1990;16:285–90. DOI: 10.1016/0272-8842(90)90041-D

[123] Xiaojuan W, Juan C, Zhiqiang S, Hua H, Lang L, Jianguo Y, Yongcun Z, Guodong L, Yongnan Z. Hydrothermal synthesis and photoluminescence properties of $BaZr_{1-x}Ti_xO3$ hollow nanospheres. Mater Lett 2012;86:21–4. http://dx.doi.org/10.1016/j.matlet.2012.07.035

[124] Ian ML, Shehan W, Clive BP. Hydrothermal synthesis and characterisation of perovskite $BaZn_{1/3}Ta_{2/3}O_3$. J Mater Chem 1999;9:2663–70.

[125] Wendelbo R, Akporiaye DE, Karlsson A, Plassen M, Olafsen A. Combinatorial hydrothermal synthesis and characterisation of perovskites. J Eur Ceram Soc 2006;26:849–59. DOI: 10.1016/j.jeurceramsoc.2004.12.031

[126] Millar CE, Wolny WW, Pardo L. Hydrothermal synthesis of modified lead titanate powders. In: Applications of Ferroelectrics, 1992. ISAF '92, Proceedings of the Eighth IEEE International Symposium on. 30 Aug–2 Sep 1992. Greenville, SC. DOI: 10.1109/ISAF.1992.300622

IntechOpen